Nuclear structure of the closed subshell nucleus ^{90}Zr studied with the $(n,n'\gamma)$ reaction

P. E. Garrett, W. Younes, J. A. Becker, and L. A. Bernstein
Lawrence Livermore National Laboratory, Livermore, California 94551, USA

E. M. Baum, D. P. DiPrete, R. A. Gatenby, E. L. Johnson, C. A. McGrath, and S. W. Yates
University of Kentucky, Lexington, Kentucky 40506-0055, USA

M. Devlin, N. Fotiades, and R. O. Nelson
Los Alamos National Laboratory, Los Alamos, New Mexico 87545, USA

B. A. Brown
Department of Physics and Astronomy and National Superconducting Cyclotron Laboratory, Michigan State University, East Lansing, Michigan 48824, USA

(Received 12 May 2003; published 25 August 2003)

States in ^{90}Zr have been observed with the $(n,n'\gamma)$ reaction using both spallation and monoenergetic accelerator-produced neutrons. A scheme comprised of 81 levels and 157 transitions was constructed concentrating on levels below 5.6 MeV in excitation energy. Spins have been determined by considering data from all experimental studies performed for ^{90}Zr. Lifetimes have been deduced using the Doppler-shift attenuation method for many of the states, and transition rates have been obtained. A spherical shell-model interpretation in terms of particle-hole excitations assuming a ^{88}Sr closed core is given. In some cases, enhancements in $B(M1)$ and $B(E2)$ values are observed that cannot be explained by assuming simple particle-hole excitations. Shell-model calculations using an extended fpg-shell-model space reproduce the spectrum of excited states very well, and the gross features of the $B(M1)$ and $B(E2)$ transition rates. Transition rates for individual levels show discrepancies between calculations and experimental values.

DOI: 10.1103/PhysRevC.68.024312 PACS number(s): 27.60.+j, 23.20.Lv, 25.40.Fq

I. INTRODUCTION

^{90}Zr is often treated as a closed subshell nucleus in shell-model calculations for the mass 90 region. With $N=50$, the neutron shell is closed, and there is a gap in the single-particle level spacing separating the $g_{9/2}$ proton orbital from the lower fp shell. However, the energy gap between the $p_{1/2}$ and $g_{9/2}$ orbitals is not so pronounced that these orbitals become completely isolated from each other. This fact is perhaps best reflected in the mixing that occurs in ^{90}Zr between the 0^+ ground state and the first-excited 0^+ state, which is also the first excited state, with the result that the ground state is described by the wave function $a(\pi p_{1/2})^2 + b(\pi g_{9/2})^2_{J=0}$ with $a=0.8$ and $b=0.6$ [1].

As the core for many calculations, ^{90}Zr has been studied in great detail by a variety of probes in order to understand its level structure. One of the most important quantities needed for shell-model calculations is the single-particle energies. These are best determined through single-nucleon-transfer reactions into the odd mass neighbors. Interaction matrix elements can be determined from detailed studies of the levels in ^{90}Zr itself, and transfer reactions have again been extensively used for this purpose: ^{91}Zr$(p,d)^{90}$Zr and ^{91}Zr$(^3$He$,\alpha)^{90}$Zr reactions [1,2] for the neutron states and for the proton states the ^{89}Y$(^3$He$,d)^{90}$Zr and ^{93}Nb$(p,\alpha)^{90}$Zr reactions [3,4].

The initial aim of this project was to measure the prompt γ-ray production cross sections induced by fast neutron bombardment of ^{90}Zr at the Los Alamos Neutron Science Center-Weapons Neutron Research (LANSCE/WNR) facility. In the analysis of the cross section data, it was found that many of the γ rays associated with the $(n,n'\gamma)$ channel could not be placed in the known level scheme. Therefore, the level scheme of ^{90}Zr had to be extended. During the course of the work, it was found that ^{90}Zr had also been studied [5] with the $(n,n'\gamma)$ reaction at the University of Kentucky, but the results had not been published. We therefore decided to combine the results from both sets of experiments; the LANSCE/WNR data had the advantage that γ-γ coincidences were recorded, while lifetimes were obtained from the Kentucky data using the Doppler-shift attenuation method. The lifetimes allowed many transition rates to be determined, providing a check on configuration assignments and a sensitive test of the shell-model calculations.

II. EXPERIMENTAL DETAILS AND RESULTS

A. Measurements using the WNR spallation source

An experiment to measure the absolute γ-ray cross sections was performed at the LANSCE/WNR facility using the germanium array for neutron-induced excitations (GEANIE) spectrometer. At the WNR facility, spallation neutrons are produced by bombarding a ^{nat}W target with 800-MeV protons from the LANSCE linac. The pulsed proton beam was delivered with a 1.8-μs spacing in 625-μs macropulses at a macropulse rate of typically 100 Hz resulting in a duty factor of 6%. The ''white'' neutron spectrum produced decreases nearly exponentially with increasing neutron energy and has a maximum energy near 800 MeV. Beam hardening materials, consisting of 1.25 cm of Pb and 1.25 cm of borated high-density polyethylene, were placed in the $60°R$ neutron flight path at $\approx$7 m from the ^{nat}W target. The neutrons were

collimated to a circular beam spot about 1.5 cm in diameter (full width at half maximum) at the scattering-sample position located 20.34 m from the neutron production target. The scattering sample consisted of 6.34 g of metallic Zr, enriched to 97.65% (as indicated by the supplier, the Isotopes Sales Division of the Oak Ridge National Laboratory). The Zr sample was disk shaped with a diameter of 2.5 cm and was placed at an angle of 109° with respect to the beam direction; the Zr sample intersected the entire neutron beam.

The scattering sample was placed at the focus of the GEANIE spectrometer, which consisted of 11 planar detectors and 1525% HPGe (high-purity Ge) coaxial detectors. All planar detectors were equipped with bismuth germanate (BGO) suppression shields, with NaI nose cones, while only nine of the coaxial detectors were equipped with BGO suppression shields. The planar detectors were arranged in rings at angles of 27.4° (four detectors), 58.4° (two detectors), 128.0° (one detector), and 142.7° (four detectors) with respect to the neutron beam direction, and γ-ray events of $E_\gamma \leqslant 1$ MeV were processed. The coaxial detectors were arranged in rings at angles of 56.6° (two detectors), 77.7° (two detectors), 100.5° (four detectors), and 129.5° (one detector), and γ-ray events were recorded up to $E_\gamma = 4$ MeV. The front faces of the Ge detectors were located at an average distance of 14.4 cm from the Zr scattering sample. Data were collected in singles-and-higher-fold mode, resulting in a total array rate of 4–5 kHz. For each event, a master gate window of 20 μs was opened during which all unsuppressed pulses from the Ge detectors were analyzed. The data stream consisted of a bit determining whether the event occurred in or out of the macropulse (i.e., in beam or out of beam), the time relative to the start of the macropulse (CLOCK, recorded in 100 ns intervals), energy E_γ, and (if in beam) time t_γ relative to the proton micropulse for each detector which indicated an event.

In the off-line analysis of the data, events were separated depending on whether they occurred in beam or out of beam. A variety of data matrices were created, including E_γ vs time-of-flight (TOF), as well as γ-γ coincidences, for the in-beam data, and E_γ vs CLOCK and γ-γ coincidences for the out-of-beam data. The collection of data between the macropulses proved to be advantageous as the spectra were rich in γ rays from well-studied β^+ and EC decays. Since the parent nuclei were produced by neutron reactions in the sample, the efficiency curve constructed from the out-of-beam data included corrections for sample attenuation and geometry effects. This enabled a detailed check of the previously determined absolute efficiency curve. The energy calibration was performed using the energies of well-known lines from the ^{90}Zr+n products. A nonlinearity polynomial was extracted by examining the deviation of the energy of a γ ray determined from a least-squares linear energy calibration from its tabulated value [6]. The energy calibration was applied to all γ rays observed from ^{90}Zr. Shown in Fig. 1 is the spectrum obtained with the coaxial Ge detectors after selecting event times corresponding to E_n=2–12 MeV neutrons. Most of the γ rays observed in this spectrum are from the ^{90}Zr$(n,n'\gamma)$ reaction. There is a large background present from neutron interactions on the Ge detector crystals

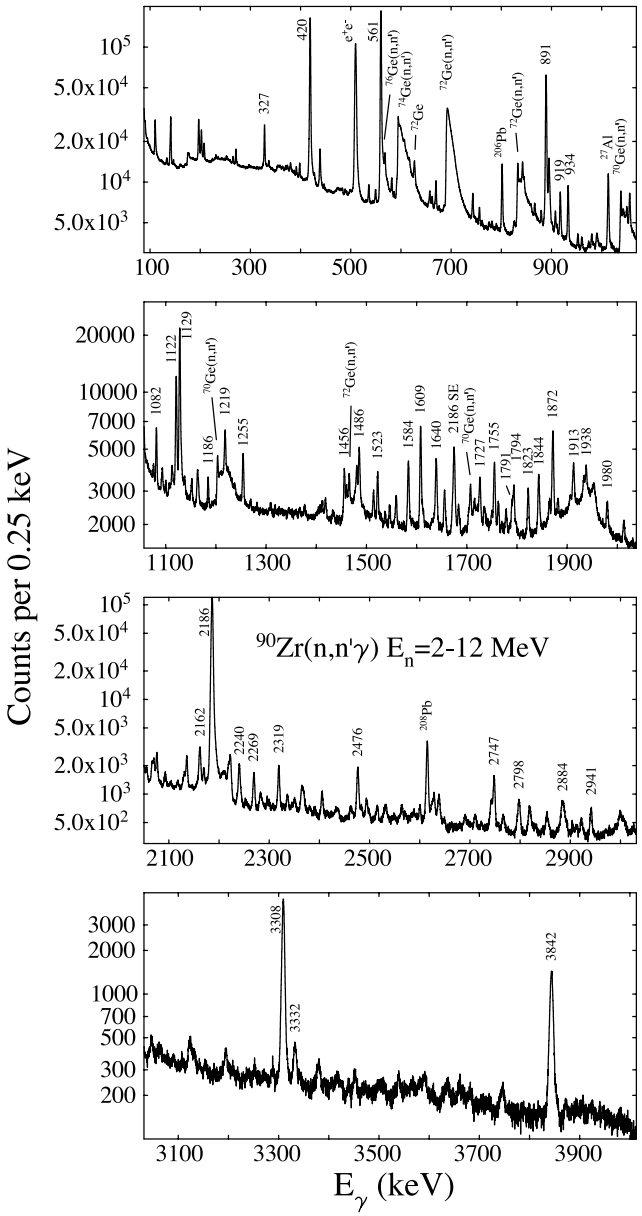

FIG. 1. Coaxial HPGe γ-ray spectrum observed with the GEANIE spectrometer and a ^{90}Zr target with the condition on the time of flight corresponding to 2–12 MeV neutrons. Some of the ^{90}Zr transitions are labeled with their energies.

that obscures ^{90}Zr γ rays in these regions.

Excitation functions were obtained by determining the yield of a particular γ ray as a function of neutron energy and dividing by the corresponding number of neutrons incident on the target, i.e.,

$$\sigma(E_\gamma,\overline{E_n}) = \frac{A_\gamma(E_\gamma,\overline{E_n})}{\epsilon_\gamma(E_\gamma)N_t(LT_\gamma)N_n(\overline{E_n})}(1+\alpha). \qquad (1)$$

The quantity $A_\gamma(E_\gamma,\overline{E_n})$ is the number of photopeak events for a γ ray of energy E_γ at a mean neutron energy $\overline{E_n}$, $\epsilon_\gamma(E_\gamma)$ is the absolute γ-ray photopeak efficiency, N_t is the target areal density of ^{90}Zr, LT_γ is the lifetime for γ-ray

detection, α is the total conversion coefficient, and $N_n(\overline{E_n})$ is the number of neutrons incident on the target at a mean energy of $\overline{E_n}$ (see below). The number of neutrons is determined using a fission chamber (see below) that is treated equally in the data acquisition system, producing more reliable results. The peak areas A_γ are found by fitting the projected spectra from the E_γ vs TOF matrix applying the time conditions $T_\gamma^L \leqslant T_\gamma < T_\gamma^H$, where $\Delta T_\gamma = T_\gamma^H - T_\gamma^L = 15$ ns, i.e., 15-ns time bins. For the purposes of the present work, the time conditions chosen correspond to a minimum neutron energy of 2 MeV and a maximum of 20 MeV. The detection time of the γ flash, prompt γ rays produced in the spallation target, was used as the reference time for the time of flight. The absolute efficiency of the array has been determined through an extensive series of measurements with calibrated γ-ray standard sources, and the relative efficiency curve obtained from the beam-off data was normalized to the absolute efficiency curve taking into account target attenuation effects. The live time for γ-ray detection was determined from the ratio of the total number of analog-to-digital (ADC) counts to the number expected from a scalar gated by the beam-on condition. The peak areas were found from a detailed fitting using the newly developed code XGAM [7] with peak shape parameters and background levels determined from a global fit to the spectrum.

The neutron flux was monitored using a fission chamber containing both ^{235}U and ^{238}U foils [9] with thicknesses of $\approx 410\ \mu g\,cm^{-2}$ and $415\ \mu g\,cm^{-2}$ located at 18.482 m and 18.495 m from the spallation source, respectively. Shown in Fig. 2 are the pulse height and TOF data from the ^{238}U fission chamber. In Fig. 2(a), the pulse height is shown as extracted for the beam-on data. The vertical line shows the lower limit taken on the pulse height in order to separate fission events from "α" events. Figure 2(b) shows the raw TOF spectrum obtained without any gating conditions on the pulse height, Fig. 2(c) with the condition that events have a pulse height corresponding to the "α" events, and in Fig. 2(d) the TOF for events with a pulse height corresponding to fission events. Included in the "α" events are those resulting from the natural α decay of ^{238}U, leading to the flat background in the TOF spectrum of Fig. 2(c), and also those originating from neutron-induced reactions on the backing material. The TOF spectrum in Fig. 2(d) is converted to a neutron intensity spectrum by using the known [10] ^{238}U (n,f) cross sections, and taking the efficiency for fission detection to be $\epsilon = 0.97$. The TOF bins correspond to the same neutron energies as the TOF bins for the γ-ray events, with the photofission events used as the reference time. The fission-chamber live time is determined by taking the ratio of beam-on ADC events to the total number as given by a scalar gated by the beam envelope.

The number of neutrons in a time bin from T^L to T^H is given by [8]

$$N_n([T^L,T^H]) = \sum_{\tau=T^L}^{T^H} N_n(\tau) \int_0^\infty \frac{1}{\sqrt{2\pi}\sigma_\tau} \times \exp\left(-\frac{(\tau-\tau')^2}{2\sigma_\tau^2}\right) d\tau', \qquad (2)$$

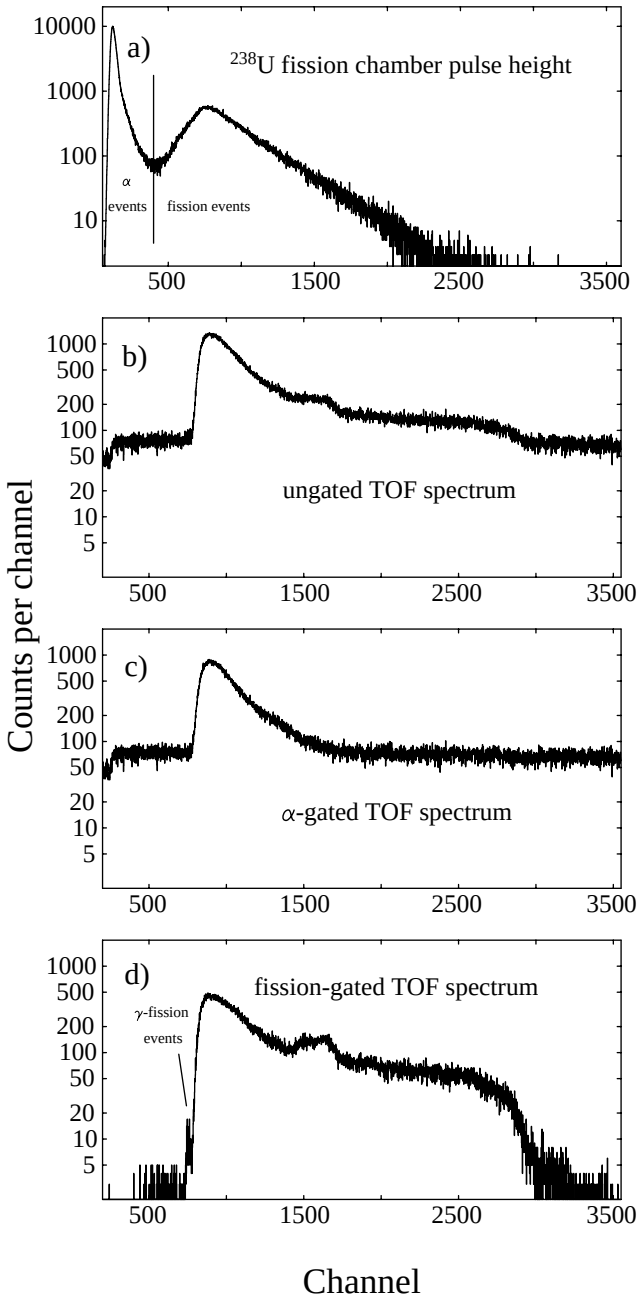

FIG. 2. Data obtained from the ^{238}U fission chamber used to determine neutron intensity at the WNR spallation neutron source. In part (a), the pulse height spectrum is shown. The vertical line corresponds to the lower limit on the pulse height for a signal to be considered a fission event. In part (b), the raw time-of-flight (TOF) spectrum is shown, defined as the time of the event in measured relative to the proton beam burst. In part (c) the TOF spectrum resulting from the condition is shown on the pulse height labeled as α events, whereas part (d) shows the TOF spectrum for fission events.

where τ is the time of flight. The effect due to the finite time resolution is taken into account and assumed to be Gaussian distributed. Since the neutron spectrum is not a constant, the mean energy $\overline{E_n}$ of the neutrons in the bin from time T^L to T^H is determined from

$$\overline{E}_n = \frac{\sum_{\tau=T^L}^{T^H} E_n(\tau) N_n(\tau) \int_0^\infty \frac{1}{\sqrt{2\pi}\sigma_\tau} \exp\left(-\frac{(\tau-\tau')^2}{2\sigma_\tau^2}\right) d\tau'}{\sum_{\tau=T^L}^{T^H} N_n(\tau) \int_0^\infty \frac{1}{\sqrt{2\pi}\sigma_\tau} \exp\left(-\frac{(\tau-\tau')^2}{2\sigma_\tau^2}\right) d\tau'} \tag{3}$$

and the variance

$$\sigma_{E_n}^2 = \frac{\sum_{\tau=T^L}^{T^H} [E_n(\tau)-\overline{E}_n]^2 N_n(\tau) \int_0^\infty \frac{1}{\sqrt{2\pi}\sigma_\tau} \exp\left(-\frac{(\tau-\tau')^2}{2\sigma_\tau^2}\right) d\tau'}{\sum_{\tau=T^L}^{T^H} N_n(\tau) \int_0^\infty \frac{1}{\sqrt{2\pi}\sigma_\tau} \exp\left(-\frac{(\tau-\tau')^2}{2\sigma_\tau^2}\right) d\tau'}. \tag{4}$$

It should be noted here that in the plots of excitation functions, examples of which are shown in Fig. 3, the horizontal E_n error bars are derived from the variance and thus represent the width of the neutron energy distribution, rather than the uncertainty on the mean neutron energy for the bin.

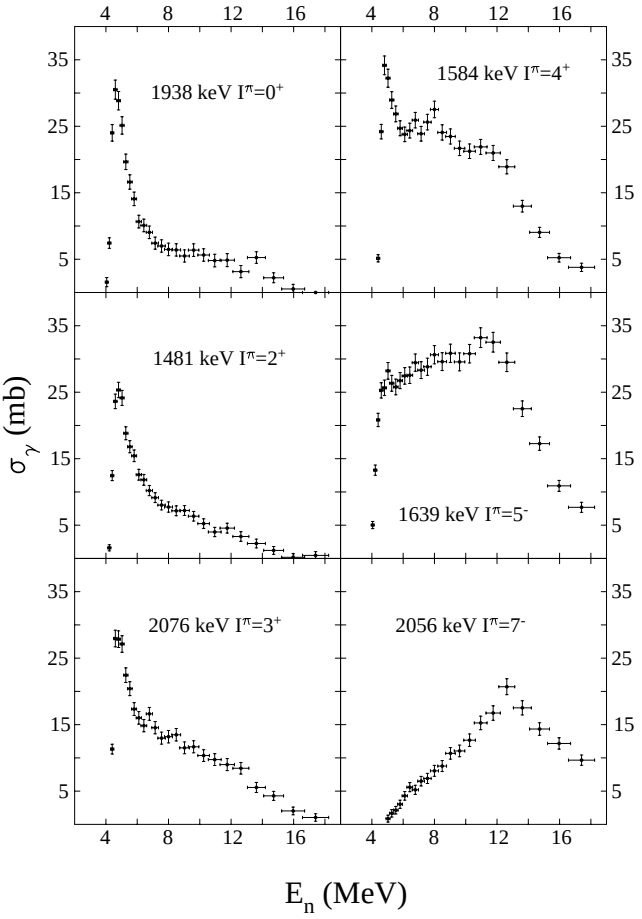

FIG. 3. Partial γ-ray cross sections obtained from GEANIE data for bombardment of a ^{90}Zr target with neutrons obtained from the WNR spallation neutron source. The excitation functions are labeled with the γ-ray energies and the initial spins. All transitions shown are newly placed.

Figure 3 illustrates excitation functions derived from the GEANIE data for selected transitions (all newly placed) with a range of initial spins. The TOF bins used to generate the data were 15 ns wide, and the ^{238}U fission chamber data were used to determine the number of neutrons. The panels are labeled by the energy of the γ ray and the spin of the initial level. As can be seen, there is an evolution in the shape of the excitation function such that, with increasing spin, the peak cross section shifts to higher energies. Therefore, the shape of the excitation function can be used to indicate the spin of the initial level. A complication arises, however, in the case of levels that experience γ-ray feeding from higher-lying states.

Multiplicity two-and-higher coincidences from both the planar and coaxial detectors were sorted into a $4k\times4k$ γ-γ matrix. Conditions were imposed on the TOF such that the time of the events had to correspond to neutron energies between 1 and 13 MeV (to minimize background from other reactions) and within $\approx$40 ns (planar detectors) or $\approx$80 ns (coaxial detectors). Figure 4 displays portions of selected coincidence spectra with some of the more prominent transitions, namely, the $2_1^+ \rightarrow 0_{\text{g.s.}}^+$ (2186 keV), the $4_1^- \rightarrow 5_1^-$ (420 keV), and the $3_1^- \rightarrow 2_1^+$ (561 keV) γ rays. The ability to establish coincidence relations, especially with the the 420- and 561-keV γ rays, allowed many transitions to be placed with confidence as feeding the 4_1^- or 3_1^- levels. The 4_1^- and 3_1^- levels are less than 9 keV apart in energy, and therefore it is impossible to place transitions that feed them based only on the excitation functions.

B. Measurements using the accelerator-produced neutrons at the University of Kentucky

A series of experiments with the aim of investigating the level structure of ^{90}Zr was performed at the University of Kentucky van de Graaff accelerator facility. The methods and techniques have been described in detail elsewhere [11,12], so only a brief outline is given here.

Neutrons are produced with either the ^{3}H$(p,n)^3$He reaction ($Q=-0.763$ MeV) or the ^{2}H$(d,n)^3$He reaction ($Q=3.270$ MeV). The first reaction is used to produce neutrons up to $\approx$5.5 MeV, whereas the second is employed to produce

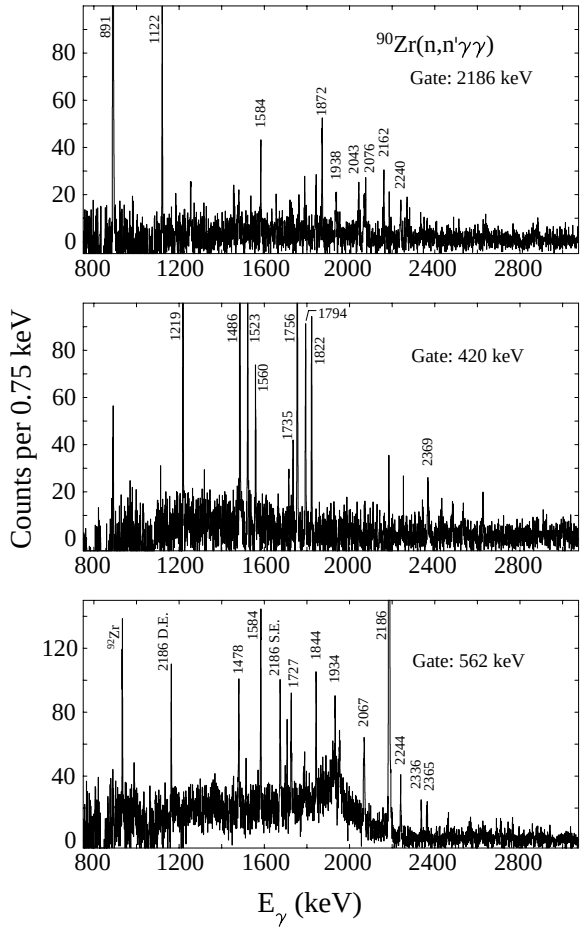

FIG. 4. Examples of γ-γ coincidence data obtained with the GEANIE array for a TOF gate corresponding to $E_n = 1-13$ MeV. Some of the more prominent γ rays are labeled with their energies.

neutrons up to ≈9 MeV. ^{3}H or ^{2}H gases were contained in cells 3.0 cm in length and 1.0 cm in diameter at a pressure of 1 and 2 atm, respectively, and separated from the beam-line vacuum by a 33-μm-thick Mo foil. Bunched beams of particles, with a pulse structure of 1.875 MHz, ≈1 ns in width, and a current of 1–2 μA, bombarded the gas cells.

The scattering sample, consisting of 50.8 g of 97.2%-enriched ^{90}Zr, was contained in a polyethylene vial 3.5 cm high and 2.8 cm diameter, suspended at 0° with respect to the beam direction and at a distance of 4.5 cm from the end of the gas cell. The sample was viewed by a HPGe detector, with 32% relative efficiency, at a distance of 104.5 cm. The detector was surrounded by an annular BGO shield for Compton suppression. This assembly was surrounded by a series of Pb rings and borated polyethylene to reduce the number of scattered neutrons and γ rays reaching the detector. Mounted forward of the detector assembly were a series of copper plates for fast-neutron shielding with a 7.5-cm central bore and a tungsten wedge so that the Ge detector had no direct view of the neutron source. Efficiency and energy calibrations were performed using radioactive sources of ^{152}Eu, ^{60}Co, ^{56}Co, as well as γ rays from the ^{35}Cl(n,γ) reaction.

Excitation function measurements were performed in 0.1-MeV steps from 3.5 to 5.0 MeV, and 0.5-MeV steps from 5.0 to 7.5 MeV, with the Ge detector positioned at an angle of 90° with respect to the beam direction. The placement of ground-state transitions above 4 MeV in energy came exclusively from the Kentucky data, because the range in γ-ray energy of data collected with the GEANIE array was limited to <4 MeV. Angular distribution measurements were performed using neutron beam energies of 5.5 and 6.5 MeV. Spectra were recorded at five angles between 30° and 145° (for $E_n = 5.5$ MeV) and between 45° and 150° (for $E_n = 6.5$ MeV). The angular distribution data were normalized to yield an isotropic distribution for γ rays from known 0^+ states. The angular distributions were fitted with the form

$$W(\theta) = I_\gamma[1 + a_2 P_2(\cos\theta_\gamma) + a_4 P_4(\cos\theta_\gamma)] \qquad (5)$$

applicable for transitions up to multipolarity two. Due to the limited number of angles, reliable information on the a_4 coefficient could not be extracted for many transitions. In the case of mixed transitions, the mixing ratio δ can be extracted when the initial spin is known. The initial m-state population distribution is assumed to be Gaussian and described by a width σ [13]. An analysis of stretched $E2$ transitions yielded an average value of $\sigma = 1.15(15)$. This value was then used in the analysis of mixed transitions, and it was further assumed that σ had no spin dependence. As such, the values of δ extracted are not expected to be very precise, but they should yield an indication of whether a transition is predominantly dipole or quadrupole in nature. Exceptions to this approach are those levels where stretched $E2$ transitions also occur with sufficient strength so that σ could be determined accurately, for example, the 3308-keV 2^+ level.

In addition to the measurement of anisotropies, the angular distribution data yielded Doppler shifts that were fitted with the expression

$$E_\gamma(\theta_\gamma) = E_\gamma^0[1 + \beta F(\tau)\cos\theta_\gamma], \qquad (6)$$

where E_γ^0 is the γ-ray energy, β is the recoil velocity in the center-of-mass frame, θ_γ is the angle of observation of the γ ray, and $F(\tau)$ is the attenuation factor. By performing a linear fit of the observed γ-ray energy as a function of $\cos\theta_\gamma$, the experimental $F(\tau)$ value can be extracted and compared with that calculated according to the formalism of Ref. [14], based on the Winterbon theory [15].

III. DISCUSSION OF THE LEVEL SCHEME

A summary of the experimental results is presented in Table I, where the level scheme has been determined using both the excitation functions and the γ-γ coincidences. In order for a γ ray to be placed based on the excitation function alone, its placement had to be unique; i.e., there could be no other choice for placement consistent with the threshold and shape of the excitation function. Also reported in Table I are the relative intensities observed for the decays from each level and the a_2 angular distribution coefficient.

To make spin-parity assignments, data from all previous experimental studies of low-lying levels in ^{90}Zr were considered. Particularly useful were experiments where charged-particle angular distributions were measured. These included

TABLE I. Level scheme for ^{90}Zr determined from the ^{90}Zr$(n,n'\gamma)$ reaction. I_{rel} represents the relative γ-ray intensity, normalized to 1.0 for each level, observed from the singles data. Uncertainties quoted for the γ-ray energies do not include an estimated 0.1 keV systematic uncertainty. The multipole mixing ratios are extracted from the a_2 coefficients assuming a Gaussian *m*-state population distribution with σ=1.15(15). If two values are given, the first has the smaller χ^2. The final column lists the new results, i.e., either a newly placed γ ray (denoted by γ) or a newly established level *L*.

E_i (keV)	I_i^π	E_γ (keV)	E_f (keV)	I_f^π	I_{rel}	a_2	δ	L/γ
1760.695(76)	0^+							
2186.205(19)	2^+	2186.224(23)	0.0	0^+	1.0	0.20(2)		
2319.019(22)	5^-	2318.956(29)	0.0	0^+	0.952(13) [a]			
		132.716(18)	1760.7	0^+	0.048(13) [a]			
2739.338(24)	4^-	420.321(13)	2319.0	5^-	1.0	0.05(2)		
2747.673(23)	3^-	429.0(3)	2319.0	5^-	0.005(1)			
		561.3(1)	2186.2	2^+	0.938(3)	−0.06(1)		
		2747.465(54)	0.0	0^+	0.057(3)	0.55(8)		
3076.816(20)	4^+	329.125(15)	2747.7	3^-	0.060(3)	−0.05(6)		
		337.8(2)	2739.3	4^-	0.008(1)			
		757.802(36)	2319.0	5^-	0.025(1)			
		890.629(14)	2186.2	2^+	0.907(3)	0.40(3)		
3308.198(29)	2^+	1121.990(22)	2186.2	2^+	0.303(26)	0.31(6)	0.25 [1.3]	
		1547.5 [b]	1760.7	0^+	0.026(7)			
		3308.1(2)	0.0	0^+	0.671(26)	0.29(3)		
3448.132(28)	6^+	1129.113(17)	2319.0	5^-	1.0	0.0(1)		
3589.309(31)	8^+	141.178(15)	3448.1	6^+	0.9810(4) [a]			
		1270.16(16)	2319.0	5^-	0.0190(4) [a]			
3842.290(91)	2^+	1656.05(11)	2186.2	2^+	0.145(13)	0.43(7)	1.1 [0.3]	γ
		3842.23(39)	0.0	0^+	0.855(13)	0.38(2)		
3958.662(33)	5^-	1219.330(30)	2739.3	4^-	0.350(8)	−0.16(7)	0.08	γ
		1639.600(39)	2319.0	5^-	0.650(8)	0.48(4)	0.06	γ
4058.117(35)	4^+	981.311(68)	3076.8	4^+	0.068(13)	0.31(23)	−0.11	γ
		1310.00(18)	2747.7	3^-	0.037(12)			γ
		1318.92(19)	2739.3	4^-	0.021(11)			γ
		1871.896(34)	2186.2	2^+	0.874(26)	0.46(5)		γ
4124.485(66)	0^+	1938.258(63)	2186.2	2^+	1.0			γ
4225.410(90)	4^-	1478.02(16)	2747.7	3^-	0.151(33)			γ
		1485.75(14)	2739.3	4^-	0.671(32)	0.54(5)	0.31	γ
		1906.50(17)	2319.0	5^-	0.178(35)	0.43(14)	−0.57	γ
4229.002(37)	2^+	1481.397(55)	2747.7	3^-	0.335(80)			γ
		2042.731(39)	2186.2	2^+	0.520(62)	0.30(8)	0.04 [2.0]	γ
		4229.3(2)	0.0	0^+	0.145(24)	0.47(7)		γ
4231.978(49)	(6^-)	1912.938(44)	2319.0	5^-	1.0	0.50(25)	0.5	
4236.973(70)	$(1,2^+)$	929.01(18)	3308.2	2^+	0.057(2)			γ
		2050.808(86)	2186.2	2^+	0.198(35)			γ
		2476.221(37)	1760.7	0^+	0.744(35)			
4262.414(32)	3^+	954.2(1)	3308.2	2^+	0.069(6)	−0.20(13)	0.06	L,γ
		1185.556(51)	3076.8	4^+	0.141(15)	0.11(20)	−3.1 [−0.2]	γ
		1514.8(1)	2747.7	3^-	0.148(25)	0.38(14)		γ
		1523.074(44)	2739.3	4^-	0.294(7)	−0.01(11)		γ
		2076.195(43)	2186.2	2^+	0.347(16)	0.44(10)	0.6	γ
4299.188(56)	(5^-)	1559.907(68)	2739.3	4^-	0.335(11)	0.30(9)	0.34	γ
		1980.058(76)	2319.0	5^-	0.665(11)	0.40(7)	0.85	γ
4331.976(32)	4^+	1255.179(32)	3076.8	4^+	0.382(11)	0.48(4)	0.1	γ
		1584.245(39)	2747.7	3^-	0.513(14)	−0.08(5)		γ
		2012.9(2)	2319.1	5^-	0.105(20)			γ
4348.106(39)	(4^+)	1608.8 [b]	2739.3	4^-	[c]			L,γ
		2161.873(34)	2186.2	2^+	1.0	−0.12(5)		γ

TABLE I. (*Continued*).

E_i (keV)	I_i^π	E_γ (keV)	E_f (keV)	I_f^π	I_{rel}	a_2	δ	L/γ
4374.809(71)	7^-	2055.765(67)	2319.0	5^-	1.0	0.31(19)		
4426.439(53)	0^+	2240.204(50)	2186.2	2^+	1.0	0.00(7)		γ
4454.751(45)	(5^+)	1377.74(12)	3076.8	4^+	0.119(22)			γ
		1715.73(14)	2739.3	4^-	0.138(50)			γ
		2135.695(45)	2319.0	5^-	0.743(51)	0.53(10)		γ
4455.617(38)	$2^{(-)}$	1707.898(53)	2747.7	3^-	0.427(25)	$-0.10(7)$	0.024	L,γ
		2269.401(44)	2186.2	2^+	0.573(25)	0.32(9)		γ
4474.369(69)	4^+	1726.678(65)	2747.7	3^-	0.713(33)			γ
		1735.1 [b]	2739.3	4^-	0.287(33)			γ
4494.846(46)	3^-	1747.2(2)	2747.7	3^-	0.047(30)			γ
		1755.489(39)	2739.3	4^-	0.953(30)	$-0.08(3)$	-0.02 [-6.4]	γ
4533.577(39)	3^-	[1225.3(2)]	3308.2	2^+	[0.104(13)]			γ
		1456.783(42)	3076.8	4^+	0.589(62)	0.54(11)		γ
		1794.153(58)	2739.3	4^-	0.227(23)	0.12(9)	2.0 [-0.4]	γ
		2347.6 [b]	2186.2	2^+	0.080(22)			γ
4537.747(47)	$4^{(-)}$	1460.951(57)	3076.8	4^+	0.385(35)			L,γ
		2218.650(69)	2319.0	5^-	0.615(35)	0.28(27)	-0.36 [-1.8]	γ
4541.465(45)	6^+	1092.97(23)	3448.1	6^+	0.075(20)			
		2222.427(40)	2319.0	5^-	0.925(20)			
4562.094(53)	5	1822.736(47)	2739.3	4^-	1.0			L,γ
4579.07(13)	$1^{(+)}$	2818.33(10)	1760.7	0^+	0.545(44)			γ
		4578.7(2)	0.0	0^+	0.455(44)	$-0.01(7)$		
4591.404(46)	3^+	1843.704(51)	2747.7	3^-	0.732(9)	0.43(6)		γ
		2405.177(73)	2186.2	2^+	0.268(9)	$-0.38(7)$	-0.07	γ
4614.428(85)	6^+	1166.24(12)	3448.1	6^+	0.401(41)			L,γ
		1537.64(12)	3076.8	4^+	0.303(41)			γ
		2295.4 [b]	2319.0	5^-	0.296(31)			γ
4640.601(51)	7,8	1051.286(40)	3589.3	8^+	1.0			
4646.7(3)	$1,2^+$	2884.8(13)	1760.7	0^+	0.845(24)			L,γ
		4646.6(3)	0.0	0^+	0.155(24)			γ
4681.469(86)	2^+	1933.774(83)	2747.7	3^-	0.506(46)			γ
		2495.2 [b]	2186.2	2^+	0.207(31)			γ
		4680.8(2)	0.0	0^+	0.286(43)	0.51(7)		γ
4701.149(87)	2^+	1953.26(17)	2747.7	3^-	0.396(18)			γ
		2514.76(13)	2186.2	2^+	0.154(11)			γ
		2940.60(12)	1760.7	0^+	0.376(17)	0.51(11)		γ
		4701.2(3)	0.0	0^+	0.074(16)	0.67(36)		γ
4774.312(84)	$(1,2)^+$	537.342(50)	4237.0	$(1,2)^+$	0.254(24)			
		2587.96(25)	2186.2	2^+	0.746(24)			
4781.87(19)	$(3^-),4$	2462.81(19)	2319.0	5^-	1.0			$L,\ \gamma$
4795.6(3)	2^+	4795.5(3)	0.0	0^+	1.0	0.48(31)		γ
4814.489(63)	3^-	2066.947(78)	2747.7	3^-	0.755(47)	0.67(26)	0.34	γ
		2495.7 [b]	2319.0	5^-	0.120(23)			γ
		2628.013(95)	2186.2	2^+	0.125(24)	$-0.02(9)$		γ
4818.080(67)	$3,4^+$	975.75(15)	3842.3	2^+	0.142(28)			L,γ
		2070.388(68)	2747.7	3^-	0.858(28)			γ
4824.32(11)	2^+	1747.2(2)	3076.8	4^+	0.06(4)			γ
		2638.07(11)	2186.2	2^+	0.801(40)	0.34(6)	0.11 [1.7]	γ
		4823.9(5)	0.0	0^+	0.139(25)	0.75(14)		γ
4840.296(66)	5^-	1763.462(63)	3076.8	4^+	0.697(36)			$L,\ \gamma$
		2092.6 [b]	2747.7	3^-	0.303(36)			γ
4867.493(67)	5^+	1419.23(10)	3448.1	6^+	0.307(34)	0.58(14)	-1.0	γ

TABLE I. (*Continued*).

E_i (keV)	I_i^π	E_γ (keV)	E_f (keV)	I_f^π	I_{rel}	a_2	δ	L/γ
		1790.733(81)	3076.8	4^+	0.588(48)	0.75(16)	0.8	γ
		2128.1 [b]	2739.3	4^-	0.105(43)			γ
4932.6(4)	$1,2^+$	4932.5(4)	0.0	0^+	1.0			L,γ
4941.861(77)	4^+	1865.025(75)	3076.8	4^+	0.757(24)			γ
		2623.0(2)	2319.0	5^-	0.243(24)			γ
4992.560(83)	2^-	1150.3 [b]	3842.3	2^+	0.166(17)			γ
		1684.345(78)	3308.2	2^+	0.554(27)	0.35(7)		γ
		2244.5(3)	2747.7	3^-	0.172(17)			γ
		2252.9(2)	2739.3	4^-	0.108(16)			γ
5060.84(12)	7^+	1612.69(11)	3448.1	6^+	1.0			
5068.6(6)	1^-	5068.4(6)	0.0	0^+	1.0			γ
5083.85(10)	$2^{(-)},(3^-)$	2336.180(97)	2747.7	3^-	0.734(45)			γ
		2345.7(3)	2739.3	4^-	0.266(45)			γ
5090.29(24)	(3^-)	2904.03(23)	2186.2	2^+	1.0			γ
5107.92(18)	$(3),4^+$	2921.66(18)	2186.2	2^+	1.0	0.51(14)		L,γ
		2368.6 [b]	2739.3	4^-				γ
5113.1(10)	3^-	2365.0(10) [d]	2747.7	3^-	1.0	0.25(11)	-0.1	γ
5171.99(13)	(4)	2432.01(30)	2739.3	4^-	0.357(33)	0.57(33)		L,γ
		2853.06(14)	2319.0	5^-	0.643(33)			γ
5175.74(32)	$3,4^+$	2989.48(32)	2186.2	2^+	1.0			L,γ
5183.61(17)	$1^+,\ 2^+$	2997.47(21)	2186.2	2^+	0.457(66)			γ
		5183.2(3)	0.0	0^+	0.543(66)			γ
5223.05(19)	4^+	2483.67(19)	2739.3	4^-	1.0	0.41(23)		γ
5232.23(30)	$3,4^+$	3045.97(30)	2186.2	2^+	1.0			L,γ
5270.82(16)	3,4	2531.44(16)	2739.3	4^-	1.0			L,γ
5305.97(20)	2^+	5305.8(2)	0.0	0^+	1.0	0.26(19)		
5307.8(2)	$3^-,4^+$	2560.2(4)	2747.7	3^-	0.097(40)			L,γ
		2988.9(2)	2319.0	5^-	0.154(31)			γ
		3121.3(2)	2186.2	2^+	0.750(47)			γ
5312.8(2)	$1,(2^+)$	(3551.4(6))	1760.7	0^+				L,γ
		5312.6(2)	0.0	0^+	1.0			γ
5317.70(26)	3^-	2570.21(36)	2747.7	3^-	0.576(67)			γ
		3131.23(36)	2186.2	2^+	0.424(67)			γ
5359.24(16)	$3^+,4$	2282.40(16)	3076.8	4^+	1.0	0.34(13)		L,γ
5379.83(25)	4^+	3193.57(25)	2186.2	2^+	1.0			γ
5426.1(2)	3^-	2118.1(2)	3308.2	2^+	0.482(86)			γ
		3106.8(2)	2319.0	5^-	0.384(66)	0.65(36)		γ
		3239.7(2)	2186.2	2^+	0.133(28)			γ
5437.79(23)	2^+	2690.08(23)	2747.7	3^-	0.618(20)	$-0.14(14)$		γ
		3676.6(2)	1760.7	0^+	0.210(17)	0.48(23)		γ
		5436.9(2)	0.0	0^+	0.180(11)	0.47(19)		γ
5457.75(16)	4^+	2380.64(28)	3076.8	4^+	0.34(11)			γ
		2710.18(20)	2747.7	3^-	0.66(11)	$-0.43(12)$		γ
5504.8(2)	1^-	3744.5(5)	1760.7	0^+	0.567(31)			
		5504.5(2)	0.0	0^+	0.433(31)			
5513.25(13)	$(3,4)^-$	2436.47(29)	3076.8	4^+	0.340(75)	$-0.21(16)$		γ
		2765.79(17)	2747.7	3^-	0.640(75)			γ
5564.20(36)	2–4	3377.93(36)	2186.2	2^+	1.0			γ
5590.6(2)	2^+	2842.9(2)	2747.7	3^-	0.181(30)			γ
		3404.1(2)	2186.2	2^+	0.523(24)			γ
		5590.9(3)	0.0	0^+	0.297(17)	0.55(14)		γ
5601.77(41)	$3,4^+$	3415.49(41)	2186.2	2^+	1.0	0.49(32)		L,γ
5607.69(29)	$3,4^+$	2299.46(29)	3308.2	2^+	1.0			L,γ

TABLE I. (*Continued*).

E_i (keV)	I_i^π	E_γ (keV)	E_f (keV)	I_f^π	I_{rel}	a_2	δ	L/γ
5651.23(30)		2911.84(30)	2739.3	4^-	1.0	0.25(18)		
5724.27(43)		3537.99(43)	2186.2	2^+	1.0	−0.22(15)		
5775.09(51)		3588.81(51)	2186.2	2^+	1.0			
5821.73(63)		3635.45(63)	2186.2	2^+	1.0			
5846.34(52)		3660.05(51)	2186.2	2^+	1.0			

[a]Branching ratio from Ref. [16].

[b]Energy of γ ray from level energy difference. Peak in singles spectrum is part of an unresolved doublet or is influenced by rapidly varying background.

[c]Branching ratio could not be determined due to contamination from a ^{209}Bi 1608.6-keV γ ray. Placement is based on the coincidence relation only.

[d]Energy from γ-ray coincidence spectra.

various inelastic scattering experiments, (p,p'), (t,t'), (α,α'), and (e,e') [17–20], single-nucleon-transfer reactions (p,d), $(^3\mathrm{He},d)$, and $(^3\mathrm{He},\alpha)$ [1,3,2], and two-nucleon transfer [21]. However, before this extensive information could be used, a correspondence between the levels observed in the present work and those in the previous studies had to be established. In some cases, this was very straightforward. In others, difficulties arose from a doublet of levels unresolved (and unknown) in the previous works, or from an apparent error in the energy calibration. In the former case, the energy resolution achieved presently, ≈2 keV for 1.3 MeV γ rays, is an order of magnitude superior to most inelastic scattering or transfer studies. In the latter case, a new energy calibration had to be applied to some of the previous data to assure that the levels corresponded to those observed in the present work. An example of this was the (p,d) results [1], where the energy scale had to be adjusted significantly.

Below, individual levels are discussed where significant new information has been obtained or new spin assignments have been determined.

1. 3958.7-keV level

While only the 11th excited state, this level had no γ-ray decays assigned to it. The I^π value of 5^- was determined previously from (p,α) and (p,p'), (α,α'), and (e,e') reactions [4,17,19,20]. The present placement of the γ ray to the 4_1^- and 5_1^- levels, the shape of the excitation functions, and the a_2 angular distribution coefficients are consistent with this assignment. A lifetime of 47 ± 9 fs is measured for this level, and the mixing ratios are consistent with almost pure dipole transitions. The $B(M1)$ values are $(0.232\pm0.045)\mu_N^2$ and $(0.178\pm0.034)\mu_N^2$ for the $5^-\rightarrow4_1^-$ and $5^-\rightarrow5_1^-$ transitions, respectively.

2. 4058.1-keV level

This level can be identified as the $(4^+, 4062\pm5)$-keV level observed in the (p,p'), (α,α'), and (e,e') studies [17,19]. The angular distribution of the 1871.9-keV γ ray has a positive a_2 coefficient as expected for a stretched quadrupole transition. The shape of the excitation function was also consistent with a spin-4 assignment. Therefore, $I^\pi=4^+$, as determined in the inelastic scattering studies, is adopted. The transition to the 2_1^+ level is enhanced with $B(E2)=7.6\pm3.1$ W.u.

3. 4225.4-, 4229.0-, and 4232.0-keV levels

A triplet of levels was observed at 4.23 MeV in (e,e') studies [20]; these states were determined to have I^π values of 2^+, 4^-, and 6^-. A peak at 4.22 MeV was also observed in the (t,t') reaction and gives a tentative $\ell=2$ assignment, although the angular distribution was rather poorly fit [18]. The (α,α') [19] and (p,t) [21] reactions also provided evidence for an $\ell=2$ transition to a level at 4.23 MeV. Levels at 4.23 MeV were populated in the (p,α) reaction and with $\ell=1$ transfer in the $(^3\mathrm{He},d)$ reaction [4,3], and finally a level at 4.22 MeV was observed with $\ell=4$ in the (p,d) reaction [1]. The present work confirms that a triplet of levels exists at this excitation energy—at 4225.4, 4229.0, and 4232.0 keV with spins 4^-, 2^+, and 6^-, respectively. The unnatural parity of the 4^- and 6^- levels explains their absence in the inelastic hadronic scattering and two-neutron-transfer studies.

4. 4262.4-keV level

This new level is established from both the excitation functions and the coincidence relations. From the large number of transitions placed as decaying from the level to final states with 2^+,3^-,4^- and 4^+, the spin is immediately restricted to be 3 or 4^+. If the level had $I^\pi=4^+$, the 1514.8-keV transition to the 3^- level would have an angular distribution with a negative a_2 coefficient, contrary to the experimental result $(a_2=0.38\pm0.14)$. Thus, a 4^+ assignment can be ruled out. If the level were a 3^- state, the 1185.6- and 2076.2-keV transitions to the 4^+ and 2^+ states, respectively, would have stretched dipole character (negative a_2), also contrary to the experimental results $(a_2=0.11\pm0.20$ and $0.44\pm0.10)$. Therefore, a 3^+ assignment, consistent with the shape of the excitation function, is adopted for the level. This spin-parity assignment is also consistent with its absence in inelastic scattering experiments and in the (p,t) reaction.

5. 4299.2-keV level

This state can be identified with a 5^- level observed at ≈4300 keV in the (e,e') reaction (see Fig. 2 of Ref. [20]). A

level was also observed at 4305-keV in the (p,p') and (α,α') studies [17,19], although in the latter case an $\ell=4$ assignment was suggested. However, the resolution obtained in the (α,α') reaction was such that this state could not be resolved from the much stronger $\ell=4$ transition to the 4^+ level at 4332 keV. The (p,α) reaction [4] populated a level with an angular distribution that appears to be a mixture of both $\ell=1$ and $\ell=3$ transitions at 4.28 MeV; this is identified as the 4299-keV level. The shape of the γ-ray excitation functions in the present experiment favor a spin of 4 or 5. The angular distributions of the decaying transitions to the 4_1^- and 5_1^- levels have positive a_2 values, ruling out 4^+ or 5^+ assignments (if positive parity, at least one of these transitions would be a stretched dipole with a negative a_2 value) and indicating negative parity. Since this level was observed in the inelastic scattering studies, a 5^- assignment is tentatively adopted.

6. 4348.0-keV level

Observed for the first time in the present work, this state decays by a 1608.8-keV γ ray to the 4_1^- level and a 2161.9-keV transition to the 2_1^+ level. While the negative a_2 coefficient for the latter γ ray would indicate that the spin changes by at most 1 unit, the shape of the excitation function definitely favors a spin-4 assignment. Therefore, a 4^+ assignment is adopted. The discrepancy with the angular distribution data suggests that the γ-ray transition to the 2_1^+ level may have some contamination (likely from ^{209}Bi); its $F(\tau)$ value is therefore also suspect.

7. 4454.8-keV level

This level is identified as the 4443-keV level observed as an $\ell=4$ transition in the ^{91}Zr(p,d) reaction [1] and the 4457-keV level observed in the $(^3\mathrm{He},\alpha)$ experiment [2]. The transfer of a $j=9/2$ neutron could populate final states with $I^\pi=2^+-7^+$. The γ-ray decay of the 4454.8-keV level populates states with 4^+, 4^-, and 5^-, thus restricting the spin to 3^-, 4, or 5. The shapes of the excitation functions are consistent with a spin-4 or -5 assignment and, combined with the transfer result, limit the I^π value to 4^+,5^+. A 4^+ assignment is inconsistent with the large positive a_2 coefficient for the transition to the 5^- level; therefore, a 5^+ assignment is adopted, in agreement with Refs. [1,2].

8. 4455.6-keV level

This new level is separated by only 0.8 keV from the previous 5^+ state; therefore, it is possible that some of the decaying transitions are common to both. However, the γ-ray energies imply that if any of the peaks are actually doublets, the unresolved member must have a rather small intensity since the Ritz combinations are satisfied well. The transitions to the 3^- and 2^+ levels limit the spins to 1^-, 2, 3, or 4^+; the shapes of the excitation functions favor a spin-2 or -3 assignment, but the angular distributions are inconsistent with a spin of 3. Therefore, a spin-2 assignment is adopted. Its absence in inelastic scattering studies favors a negative-parity assignment.

9. 4533.6-keV level

Transitions to the 2_1^+, 4_1^+, and 4_1^- states, with a tentative decay to the 2_2^+ level, were observed to have thresholds of 4.5 MeV, establishing a level at 4533.6 keV. The spin is limited to the range 3–4 based on these decays. The angular distributions for these transitions are not conclusive. However, the shapes of the excitation functions favor a spin-3 assignment. With this assignment, the angular distribution of the transition to the 4^- level implies a mixed $E2/M1$ multipolarity, thus yielding a negative-parity assignment. This level is identified as the 4540-keV level observed in the (p,α) reaction [4] with an $\ell=1$ transition.

10. 4537.7-keV level

This new level decays to the 4_1^+ and 5_1^- states. The decaying transitions restrict the spin range to 3^-, 4, 5, or 6^+, while the shapes of the excitation functions favor a spin-4 assignment. While not conclusive, the angular distribution for the transition to the 5^- level favors a mixed $E2/M1$ multipolarity, implying negative parity for the 4537.7-keV level.

11. 4562.1-keV level

This new level decays by a sole transition of 1822.8 keV to the 4_1^- state. The angular distribution of this γ ray has a negative a_2 coefficient, indicating that the spin difference is at most one unit. The shape of the excitation function favors a spin-5 assignment. There may be evidence of a 2243-keV transition to the 5_1^- level as well, as the peak from a much stronger 2240-keV transition appears to have a ''shoulder'' on its high-energy side. However, the excitation function for this additional peak is inconclusive.

12. 4579.1-keV level

A spin-1 state was observed in the (γ,γ') experiments [23] at 4580 ± 2 keV, and the ground-state transition as well as a more intense γ-ray decay to the 0_2^+ level are observed in the present work. This level is suggested to be the 4.56 ± 0.02 MeV state populated in the $(^3\mathrm{He},d)$ reaction [3] with an $\ell=1$ transition. Since the ^{89}Y target has $I^\pi=1/2^-$, the 4579.1-keV level is assigned as having positive parity.

13. 4591.4-keV level

This level was suggested previously to be a 3^+ level based on the strength observed in the (p,d) reaction (although that work placed the level at 4578 keV) [1]. The angular distributions of the γ rays placed as decaying from this level in the present work are indicative of dipole transitions, and the excitation functions are consistent with a spin-3 state. Therefore, the previous 3^+ assignment is adopted here.

14. 4614.8-keV level

Transitions with energies of 1166.2, 1537.6, and 2295.4 keV are observed with thresholds of $\approx$4.7 MeV. These γ rays decay to 4^+, 5^-, and 6^+ levels, establishing a new

level at 4615 keV and limiting the spin to 4^+, 5, or 6^+. The shapes of the excitation functions are consistent with spin 6 only. Therefore, a 6^+ assignment is adopted.

15. 4781.9-keV level

This new level is observed to decay to the 5_1^- level only. Its spin is therefore restricted to the range 3–7. The excitation function, while not conclusive, favors a spin-3 or -4 assignment. If the level were 3^-, an unlikely large $B(E2)$ value of 19 W.u. for the transition would result. Therefore, a spin of 4 is favored.

16. 4795.6-keV level

Identified with the 4.78(2)-MeV level observed in the (p,α) reaction [4], this level decays by a sole transition to the ground state. The positive a_2 coefficient implies a 2^+ assignment.

17. 4818.1-keV level

A new level is established at 4818.1 keV, with decay branches to the 3842.3-keV 2^+ and the 2747.7-keV 3^- levels. The spin value is thus 1^-, 2, 3, or 4^+. The shape of the excitation function strongly favors a spin-3 or -4 assignment. The angular distributions did not yield a statistically significant a_2 value.

18. 4840.3-keV level

This new level decays to the 4_1^+ and 3_1^- levels, limiting the possible I^π values to be 2^+, 3, 4, or 5^-. The shape of the excitation function is inconsistent with spin 3 or 4, but is consistent with spin 5. Therefore, a 5^- assignment is adopted.

19. 4867.5-keV level

This level can be associated with the 4875-keV state observed in the (p,p') reaction [17]. The decay pattern limits the spin to the range 4^+, 5, while the shape of the excitation function favors a spin-5 assignment. Assuming this spin, the angular distributions of the transitions to the 4^+ and 6^+ levels are inconsistent with pure dipole multipolarity, as would be the case for the 5^- assignment. Therefore, 5^+ is adopted.

20. 4992.6-keV level

This level can be associated with the 4980-keV level observed in the (p,d) reaction populated with an $\ell=1$ transfer. Since the ^{91}Zr target ground-state spin is $5/2^+$, an $\ell=1$ transfer transition could populate levels with spins in the range $1^- - 4^-$. This level is also identified as being populated in the $(^3\mathrm{He},d)$ reaction [3] with an $\ell=2$ transition, limiting the spin/parity range to $1^- - 3^-$. The decaying transitions from this level populate final states with spins 2^+, 3^-, and 4^-. Combined with the transfer results, 2^- or 3^- are the only possibilities. The only reliable angular distribution that could be extracted was obtained for the 1684-keV transition to the 2^+ level, which must be a pure dipole transition. Since its a_2 coefficient is positive, only a 2^- assignment is consistent with all the data.

21. 5083.9-keV level

This level, identified as one part of a doublet populated by an $\ell=2$ transition in the $(^3\mathrm{He},d)$ reaction [3], and hence having negative parity, decays by two transitions to the 3_1^- and 4_1^- levels. From the shape of the excitation functions, the spin can be restricted to either 2 or 3, although a spin of 2 is favored.

22. 5090.3-keV level

This level is identified as the other part of the doublet populated with an $\ell=2$ transition in the $(^3\mathrm{He},d)$ reaction [3]. The shape of the excitation function indicates a spin of 3. Therefore, a 3^- assignment is tentatively adopted. The negative a_2 angular distribution coefficient for the transition to the 2_1^+ level is consistent with this assignment.

23. 5107.9-keV level

This new level decays to the 2_1^+ and 4_1^- states, yielding possible I^π values of 2^-, 3, or 4^+. The shape of the excitation function and the positive a_2 value for the transition to the 2_1^+ level are consistent with a 4^+ assignment; however, a spin of 3 cannot be ruled out.

24. 5172.0-keV level

This new level decays to both the 4_1^- and 5_1^- levels. The shape of the excitation function favors a spin-4 assignment. The angular distribution for the 2432-keV γ ray has a positive a_2 coefficient, consistent with a $\Delta I=0$ dipole transition to the 4^- state.

25. 5175.7-keV level

A new level is established by a sole transition of 2989.5 keV to the 2_1^+ state. From the shape of the excitation function, a spin of 3 or 4 is suggested. No useful information to further restrict the spin value was obtained from the angular distributions.

26. 5183.6-keV level

Identified with the 5180-keV level observed in the $(^3\mathrm{He},d)$ reaction [3], this level decays to the 0^+ ground state as well as the 2_1^+ level. This decay pattern limits the spin to 1 or 2^+. It is populated with an $\ell=1$ transition in the $(^3\mathrm{He},d)$ reaction [3], implying that it has positive parity.

27. 5359.2-keV level

This new level was observed in the present work to decay by a single transition to the 4_1^+ state, restricting the spin to 2^+, 3, 4, 5, or 6^+. The excitation function for the 2282-keV γ ray favors a spin assignment of either 3 or 4. The positive a_2 coefficient further rules out negative parity if the spin is 3.

IV. CONFIGURATION ASSIGNMENTS

A wealth of complementary data are available on ^{90}Zr and is helpful not only for level assignments but also for configuration assignments [24–27]. Especially useful in this regard are the results from transfer reactions, summarized in Fig. 5, and the inelastic scattering studies. To these data, the results of the present work add γ-ray branchings and, in many cases, transition rates or limits as given in Table II. In this section, suggested dominant components in the wave functions will be given for many of the low-lying levels. These suggested configurations should not be viewed as being pure (there can be a large degree of mixing of the configurations), but rather reflect the components that are sampled by the variety of probes. Many of these assignments have been given in various other papers, but these tended to concentrate on comparisons with the specific experimental data. In this study, the results from all available data on ^{90}Zr have been used in order to suggest configuration assignments.

Since ^{90}Zr has a closed $N=50$ neutron shell and closed $Z=40$ proton subshell, it can be expected that the low-lying levels can be approximated as simple particle-hole excitations. For the present discussion, ^{88}Sr, with its closed $N=50$ neutron shell and $p_{3/2}$ and $f_{5/2}$ proton subshells, is taken as the core. The suggested dominant wave function components are summarized in Fig. 6.

A. The $(\pi p_{1/2})^2+(\pi g_{9/2})^2$ configuration

For spherical shapes, the $Z=40$ Fermi surface lies between the $p_{1/2}$ and $g_{9/2}$ orbitals. Since both can couple to form $I^\pi=0^+$ states, it is expected that a 0^+ state occurs at low-excitation energies in addition to the ground state in ^{90}Zr. This is indeed the case, and it has been demonstrated (see, e.g., Ref. [32]) that these configurations mix appreciably. From the ^{89}Y(^{3}He,d) reaction [3], the target ground state of which has the $p_{1/2}$ configuration, the spectroscopic factor for the transfer of the $p_{1/2}$ proton to the ground state and the first-excited 0^+ state at 1761 keV are $(2j+1)C^2S=1.31$ and 0.52, respectively. The ground-state wave function, when written as $|0^+_{\text{g.s.}}\rangle=a(\pi p_{1/2})^2+b(\pi g_{9/2})^2$, has $a\approx 0.8$ and $b\approx 0.6$ [1], or is almost completely mixed. The remaining states from the $(\pi g_{9/2})^2$ coupling– 2^+, 4^+, 6^+, and 8^+–are then expected to form the yrast band, as observed in Fig. 6. All experimental studies are consistent with these states having a predominantly $(\pi g_{9/2})^2$ configuration, as most recently demonstrated with the g-factor measurement of the 2_1^+ level [33]. However, the large $B(E2)$ values for the transitions in the yrast band, most notably $B(E2;2_1^+\rightarrow 0_1^+)$ of 5.2 ± 1.0 W.u., indicates a certain degree of collectivity in the wave function. A folding-model analysis using

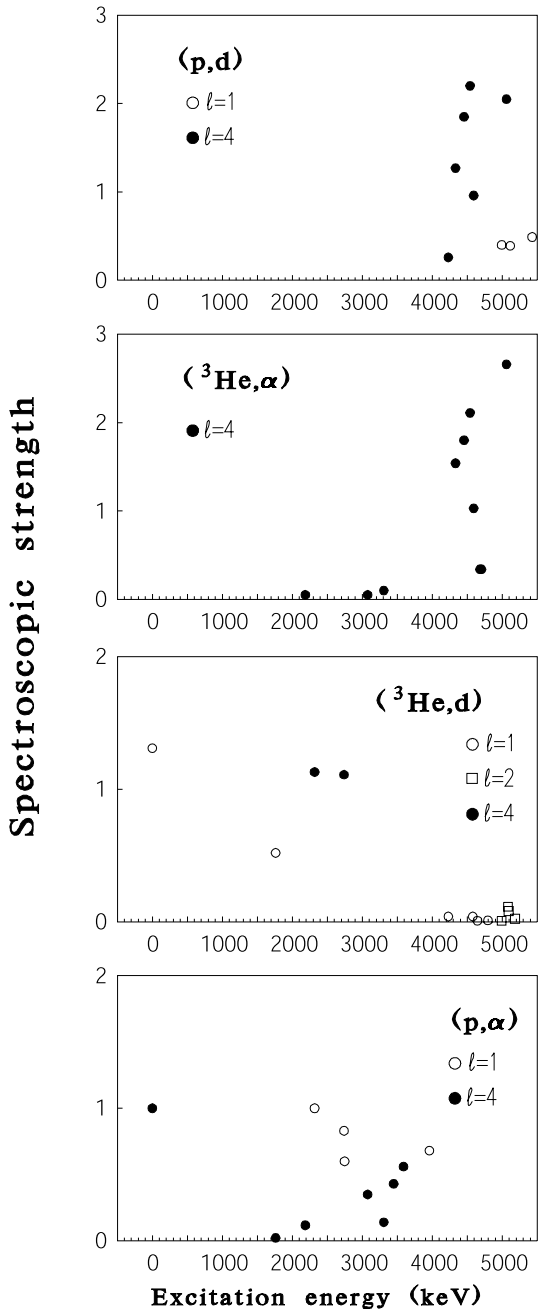

FIG. 5. Summary of results from nucleon-transfer reactions into ^{90}Zr [1–4]. The panels are labeled with the reaction used. Only results up to 5.5 MeV, and those where the transfer peak could be identified with a level observed in the present work, are shown. The (p,d), $(^3\text{He},\alpha)$, $(^3\text{He},d)$, and (p,α) data are taken from Refs. [1–4], respectively.

Bohr-Mottelson collective transition densities for the 2^+ level (α,α') data indicated that, while the deduced value of 1.04 ± 0.13 for the M_n/M_p ratio was smaller than the N/Z ratio of 1.25, it was larger than the value of 0.84 from random-phase approximation calculations [35], suggesting an isoscalar contribution to the wave function. This contribution, however, must be rather small since the g factor is in excellent agreement with that expected for a pure $(\pi g_{9/2})^2$ configuration [33].

TABLE II. Transition rates for γ-ray decays in ^{90}Zr determined from the ^{90}Zr$(n,n'\gamma)$ reaction, or taken from Ref. [16]. For the cases of mixed $E2/M1$ transitions, the δ values are taken from Table I. Values in brackets are calculated using the second possible solution for δ.

E_i (keV)	$F(\tau)$	τ (fs)	I_i^π	E_f (keV)	I_f^π	$B(E1)$ ($\times 10^{-3}$ W.u.)	$B(E2)$ (W.u.)	$B(M1)$ (μ_N^2)
1760.7		88.4(36) ns [a]	0^+	0.0	0^+		$\rho^2(E0)\times 10^3 = 3.3(17)$ [b]	
2186.2		127(4) [a]	2^+	1760.7	0^+		5.2(10) [a]	
				0.0	0^+		5.37(18)	
2319.0		1167(4) ms [a]	5^-	0.0	0^+		$B(E5) = 8.7(4)$ W.u. [a]	
				2186.3	2^+		$B(E3) = 0.18(6)$ W.u. [a]	
2747.7		6.8(9) ps [c]	3^-	2319.0	5^-		1.7(4)	
				2186.2	2^+	0.38(5)		
				0.0	0^+		$B(E3) = 26(3)$ W.u. [c]	
3308.2	0.29(5)	140^{+40}_{-30}	2^+	2186.2	2^+		2.7(7) [28(8)]	0.088(25) [0.035(10)]
				1760.7	0^+		0.77(29)	
				0.0	0^+		0.44(12)	
3448.1	0.01(1)	>2100	6^+	3076.9	4^+		<44	
				2319.0	5^-	<0.16		
3589.3		189(6) ns [a]	8^+	3448.1	6^+		2.40(16)	
				2319.0	5^-		$B(E3) = 0.052(3)$ W.u.	
3842.3	0.61(4)	35(7)	2^+	2186.2	2^+		6.2(14) [0.9(2)]	0.023(5) [0.048(10)]
				0.0	0^+		0.99(20)	
3958.7	0.54(5)	47(9)	5^-	2739.3	4^-		0.6(1)	0.232(45)
				2319.0	5^-		0.14(3)	0.178(34)
4058.1	0.23(7)	170^{+90}_{-50}	4^+	3076.8	4^+		0.18(8)	0.024(11)
				2747.7	3^-	0.047(25)		
				2739.3	4^-	0.026(17)		
				2186.2	2^+		7.6(31)	
4225.4	0.67(6)	29(7)	4^-	2747.7	3^-		$<25(8)$	$<0.092(30)$
				2739.3	4^-		9.5(23)	0.37(9)
				2319.0	5^-		2.0(6)	0.038(12)
4229.0	0.59(3)	39(4)	2^+	2747.7	3^-	1.3(3)		
				2186.2	2^+		0.020(3) [10.2(16)]	0.089(14) [0.018(3)]
				0.0	0^+		0.093(18)	
4232.0	0.46(15)	65^{+53}_{-28}	(6^-)	2319.0	5^-		$4.1^{+3.1}_{-1.8}$	$0.10^{+0.08}_{-0.04}$
4237.0	0.26(4)	150(30)	$(1,2^+)$	3308.2	2^+			
				2186.2	2^+			
				1760.7	0^+			
4262.4	0.11(3)	400^{+190}_{-100}	3^+	3308.2	2^+		0.027(9)	0.011(4)
				3076.8	4^+		4.6(16) [0.20(6)]	0.0011(4) [0.012(4)]
				2747.7	3^-	0.052(19)		
				2739.3	4^-	0.10(3)		
				2186.2	2^+		0.20(7)	0.0041(14)
4299.2	0.56(6)	44(9)	(5^-)	2739.3	4^-		2.9(6)	0.102(21)
				2319.0	5^-		7.1(15)	0.064(13)
4332.0	0.50(4)	54(9)	4^+	3076.8	4^+		0.77(13)	0.202(34)
				2747.7	3^-	1.2(2)		
				2319.1	5^-	0.16(3)		
4348.1	(0.57(8))	(42(10))	(4^+)	2739.3	4^-			
				2186.2	2^+		$<17(4)$	
4426.4	0.15(8)	290^{+340}_{-110}	0^+	2186.2	2^+		$2.1^{+1.3}_{-1.1}$	
4455.6	0.20(4)	200^{+70}_{-40}	$2^{(-)}$	2747.7	3^-		$0.0029^{+0.0005}_{-0.0008}$	$0.024^{+0.004}_{-0.006}$
				2186.2	2^+	0.012(3)		
4474.4	0.19(10)	220^{+260}_{-90}	4^+	2747.7	3^-	$0.31^{+0.21}_{-0.14}$		
				2739.3	4^-	$0.12^{+0.08}_{-0.07}$		
4494.8	0.47(5)	61(11)	3^-	2747.7	3^-		$<1.6(10)$	$<0.008(5)$
				2739.3	4^-		0.013(2) [31(6)]	0.16(3) [0.0039(7)]

TABLE II. (*Continued*).

E_i (keV)	$F(\tau)$	τ (fs)	I_i^π	E_f (keV)	I_f^π	$B(E1)$ ($\times 10^{-3}$ W.u.)	$B(E2)$ (W.u.)	$B(M1)$ (μ_N^2)
4533.6	0.37(11)	100^{+50}_{-40}	3^-	3308.2	2^+	0.26(12)		
				3076.8	4^+	0.93(43)		
				2739.3	4^-		3.3(15) [0.57(26)]	0.0045(21) [0.019(9)]
				2186.2	2^+	0.030(16)		
4537.7	0.22(7)	190^{+100}_{-65}	$4^{(-)}$	3076.8	4^+	$0.31^{+0.16}_{-0.11}$		
				2319.0	5^-		$<2.1^{+1.1}_{-0.7}$	$<0.017^{+0.009}_{-0.006}$
4541.5	0.39(7)	85^{+24}_{-18}	6^+	3448.1	6^+		<19(7)	<0.038(14)
				2319.0	5^-	0.48(11)		
4562.1	0.20(7)	200^{+140}_{-60}	5	2739.3	4^-			
4579.1	0.89(4)	7.4(2.9)	$1^{(+)}$	1760.7	0^+			0.19(7)
				0.0	0^+			0.036(15)
4591.4	0.21(4)	200^{+60}_{-40}	3^+	2747.7	3^-	0.28(7)		
				2186.2	2^+		0.19(5)	0.0037(9)
4646.7	0.90(11)	7(6)	$1,2^+$	1760.7	0^+			
				0.0	0^+			
4681.5	0.56(6)	44(10)	2^+	2747.7	3^-	0.77(19)		
				2186.2	2^+		<1.7(5)	<0.017(5)
				0.0	0^+		0.10(3)	
4701.1	0.45(4)	66(10)	2^+	2747.7	3^-	0.39(6)		
				2186.2	2^+		<0.79(13)	<0.008(1)
				1760.7	0^+		0.88(14)	
				0.0	0^+		0.017(4)	
4781.9	0.75(23)	20^{+32}_{-19}	$(3^-),4$	2319.0	5^-			
4795.6	0.85(8)	10^{+8}_{-5}	2^+	0.0	0^+		1.1(7)	
4818.1	0.21(12)	200^{+280}_{-100}	$3,4^+$	3842.3	2^+			
				2747.7	3^-			
4824.3	0.49(6)	58^{+15}_{-12}	2^+	3076.8	4^+		2.2(15)	
				2186.2	2^+		$0.044^{+0.012}_{-0.009}$ [$2.7^{+0.7}_{-0.5}$]	$0.042^{+0.011}_{-0.009}$ [$0.011^{+0.003}_{-0.002}$]
				0.0	0^+		0.031(10)	
4840.3	0.30(7)	120^{+40}_{-20}	5^-	3076.8	4^+	$0.51^{+0.11}_{-0.13}$		
				2747.7	3^-		$2.1^{+0.5}_{-0.6}$	
4867.5	0.21(5)	200^{+70}_{-50}	5^+	3448.1	6^+		$4.5^{+1.6}_{-1.3}$	$0.015^{+0.005}_{-0.004}$
				3076.8	4^+		$2.1^{+0.7}_{-0.6}$	$0.018^{+0.006}_{-0.005}$
				2739.3	4^-	$0.026^{+0.014}_{-0.013}$		
4932.6	0.16(11)	260^{+}_{-160}	$1,2^+$	0.0	0^+			
4941.9	0.44(6)	70(15)	4^+	3076.8	4^+		<16(4)	<0.09(2)
				2319.0	5^-	0.09(2)		
4992.6	0.14(5)	300^{+180}_{-80}	2^-	3842.3	2^+	0.18(7)		
				3308.2	2^+	0.19(7)		
				2747.7	3^-		<0.34(13)	<0.003(1)
				2739.3	4^-		<0.21(9)	<0.002(1)
5068.6	0.85(18)	10^{+19}_{-9}	1^-	0.0	0^+	$0.37^{+3.36}_{-0.24}$		
5083.8	0.46(8)	66^{+18}_{-14}	$2^{(-)},(3^-)$	2747.7	3^-			
				2739.3	4^-			
5107.9	0.37(12)	100^{+60}_{-40}	$(3),4^+$	2186.2	2^+		$1.6^{+1.1}_{-0.6}$	
				2739.3	4^-			
5172.0	0.64(8)	33^{+11}_{-9}	(4)	2739.3	4^-			
				2319.0	5^-			
5175.7	0.65(11)	32^{+30}_{-12}	$3,4^+$	2186.2	2^+			
5183.6	0.85(6)	10(5)	$1^+,2^+$	2186.2	2^+			
				0.0	0^+			
5232.2	0.59(4)	49(4)	$3,4^+$	2186.2	2^+			
5270.8	0.70(33)	24^{+76}_{-23}	3,4	2739.3	4^-			

TABLE II. (*Continued*).

E_i (keV)	$F(\tau)$	τ (fs)	I_i^π	E_f (keV)	I_f^π	$B(E1)$ ($\times 10^{-3}$ W.u.)	$B(E2)$ (W.u.)	$B(M1)$ (μ_N^2)
5306.0	0.69(5)	25(7)	2^+	0.0	0^+		0.32(9)	
5307.8	0.32(13)	105^{+115}_{-35}	$3^-,4^+$	2747.7	3^-			
				2319.0	5^-			
				2186.2	2^+			
5312.8	0.39(6)	85(15)	$1,(2^+)$	1760.7	0^+			
				0.0	0^+			
5317.7	0.15(5)	280^{+160}_{-80}	3^-	2747.7	3^-		$<0.63^{+0.26}_{-0.24}$	$<0.0069^{+0.0029}_{-0.0026}$
				2186.2	2^+	0.024(10)		
5359.2	0.64(4)	33(5)	$3^+,4$	3076.8	4^+			
5379.8	0.67(5)	29(6)	4^+	2186.2	2^+		3.5(7)	
5426.1	0.42(9)	75^{+28}_{-20}	3^-	3308.2	2^+	$0.33^{+0.13}_{-0.11}$		
				2319.0	5^-		$0.60^{+0.24}_{-0.19}$	
				2186.2	2^+	$0.025^{+0.011}_{-0.009}$		
5437.8	0.61(3)	35(5)	2^+	2747.7	3^-	0.44(6)		
				1760.7	0^+		0.30(5)	
				0.0	0^+		0.037(6)	
5457.7	0.73(3)	23(4)	4^+	3076.8	4^+		$<6.9(26)$	$<0.065(24)$
				2747.7	3^-	0.73(18)		
5504.8	0.85(2)	11(1)	1^-	1760.7	0^+	0.47(5)		
				0.0	0^+	0.11(1)		
5513.2	0.18(8)	230^{+110}_{-80}	$(3,4)^-$	3076.8	4^+			
				2747.7	3^-			
5564.2	0.87(6)	11(4)	2–4	2186.2	2^+			
5590.6	0.73(2)	23(3)	2^+	2747.7	3^-	0.17(4)		
				2186.2	2^+		$<1.7(2)$	$<0.033(4)$
				0.0	0^+		0.081(11)	
5601.8	0.61(4)	35(6)	$3,4^+$	2186.2	2^+			
5607.7	0.76(12)	20^{+13}_{-10}	$3,4^+$	3308.2	2^+			
5651.2	0.50(5)	65(7)		2739.3	4^-			
5724.3	0.63(5)	32(6)		2186.2	2^+			
5775.1	0.61(10)	35^{+30}_{-8}		2186.2	2^+			
5846.3	0.75(35)	20^{+63}_{-19}		2186.2	2^+			

[a]From Ref. [16].

[b]From Ref. [28].

[c]Calculated using $B(E3)\uparrow = 0.087(10)\ e^2\ b^3$ from Ref. [29]. The lifetime listed in Ref. [16] used $B(E3)\uparrow = 0.027(5)\ e^2\ b^3$ from (^{17}O,^{17}O$'$) data [30]. However, it has been shown [31] that a folding-model analysis of the (^{17}O,^{17}O$'$) data provides a superior fit of the angular distributions and results in $B(E3)\uparrow = 0.071\ e^2\ b^3$.

Assuming a pure j^2 configuration, the $B(E\lambda)$ values within the band are given by

$$B(E\lambda; I_i^\pi \rightarrow I_f^\pi) = 4(2j+1)(2I_f+1) \times \begin{Bmatrix} j & j & I_i \\ \lambda & I_f & j \end{Bmatrix}^2 |\langle \phi_j \| \mathcal{T}_\lambda^E \| \phi_j \rangle|^2, \quad (7)$$

where $|\phi_j\rangle$ is the single-particle wave function, $\{\}$ indicates a $6j$ symbol, and $\mathcal{T}_\lambda^E$ is the transition operator. The ratios of the $B(E2)$ values within the band are thus given solely by ratios of spin factors. With the wave function for the 0_2^+ level determined from single-nucleon-transfer studies [1] of $0.8(\pi g_{9/2})^2 - 0.6(\pi p_{1/2})^2$, the $B(E2;8^+ \rightarrow 6^+)/B(E2;2^+ \rightarrow 0_2^+)$ ratio is predicted to be 0.497, in excellent agreement with the experimental value of 0.46 ± 0.09. Unfortunately, the $B(E2)$ values for the other members of the $(\pi g_{9/2})^2$ configuration could not be determined in the present study, but Fig. 7 shows the expected values based on Eq. (7). Also shown are the values for the $2_1^+ \rightarrow 0_{\text{g.s.}}^+$ decay, where it can be seen that the decay to the ground state is stronger than that predicted using the wave function $0.8(\pi p_{1/2})^2 + 0.6(\pi g_{9/2})^2$. This effect may be related to collective components in the 2_1^+ wave function not taken into account here.

B. The $\pi p_{1/2} \pi g_{9/2}$ configuration

The breaking of a $p_{1/2}$ pair and promotion of one of the particles into the $g_{9/2}$ orbital results in the coupling of these two orbitals to form 4^- and 5^- levels that should occur at

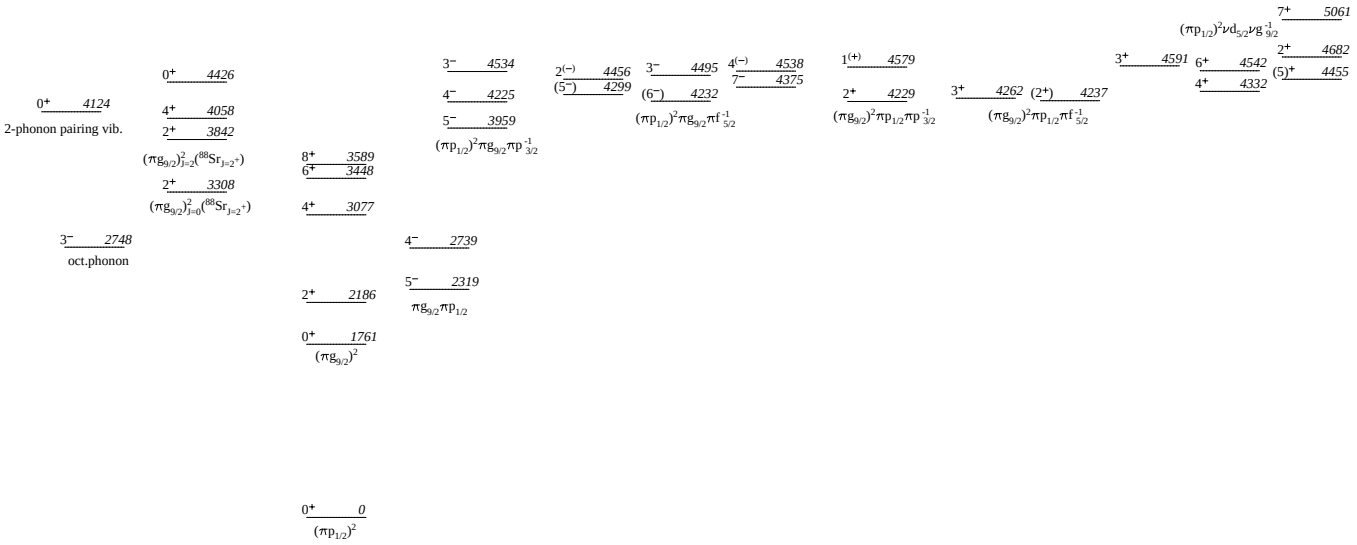

FIG. 6. Interpretations of selected levels in ^{90}Zr in terms of simple shell-model configurations. Only the dominant wave function components are given with ^{88}Sr used as the core.

low energy in ^{90}Zr. These states have been observed, the lower of the two, the 5^- level at 2319 keV, is an isomeric state that decays by an $E5$ transition to the ground state and an $E3$ transition to the 2_1^+ level. The $B(E5;5^- \rightarrow 0^+_{\text{g.s.}})$ value is 8.7 ± 0.4 W.u., indicating some degree of collectivity in this 5^- level. In fact, it has recently been suggested [34] that the lowest 5^- levels in the $Z=40-50$ region are collective one-phonon (diatriacontapolar) excitations. Evidence for this interpretation comes from the near constancy of their excitation energies and large deformation parameters β_5 [36]. Moreover, these states are significantly populated in many transfer studies such as one- and two-neutron-transfer reactions, a behavior not expected for pure proton excitations. However, results from single-proton transfer studies, as illustrated in Fig. 5, show that the wave function is dominated by the $\pi p_{1/2} \pi g_{9/2}$ configuration, and it is labeled as such. The 4^- member, located at 2739 keV, is shown convincingly in single-proton transfer studies [3,4].

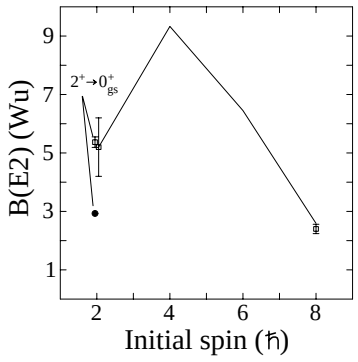

FIG. 7. $B(E2)$ values for decaying transitions within the $(\pi g_{9/2})^2$ configuration. The bold line joins the predicted values using Eq. (7) and the $2_1^+ \rightarrow 0_2^+$ transition to determine the transition matrix element. The values slightly to the left of spin 2 are for the decay to the ground state, where the filled circle is the predicted value.

C. The octupole phonon

The lowest 3^- level at 2748 keV has a large $B(E3;3^- \rightarrow 0^+_{\text{g.s.}})$ value of 26 ± 3 W.u. as determined from (e,e') studies [20]. The inelastic scattering studies of Ref. [35] indicated that this was an isoscalar excitation, with an M_n/M_p ratio of 1.31 ± 0.11 in excellent agreement with $N/Z=1.25$. This observation is taken as strong evidence for the octupole phonon nature of the 3_1^- level.

At about twice the 3^- energy, in the vicinity of 5.5 MeV, it may be expected that two-phonon octupole excitations should occur. These would form a quadruplet of states with spin parities 0^+, 2^+, 4^+, and 6^+. While in a region of increasing level density, it may be possible that enough of the collective natures of these levels are retained to be observed in highly sensitive Coulomb excitation experiments.

D. Excitations of the ^{88}Sr core

The lowest 2^+ in ^{88}Sr, occurring at 1836 keV, has a rather large $B(E2;2^+ \rightarrow 0^+_{\text{g.s.}}) = 7.2 \pm 0.2$ W.u. [22] indicative of the collective nature of the wave function. Detailed calculations support this notion [37], and list the main amplitudes as $\pi p_{3/2}^{-1} \pi p_{1/2}$ and $\pi f_{5/2}^{-1} \pi p_{1/2}$, with $\approx 20-30\%$ of the wave function consisting of neutron $1p$-$1h$ contributions. The substantial occupancy of the $\pi p_{1/2}$ orbital in the 2_1^+ wave function implies that one should consider any core excitation in ^{90}Zr as coupling to the $g_{9/2}$ proton pair, with the $(\pi g_{9/2})^2_{J=0^+} \otimes {}^{88}\text{Sr}_{2^+}$ lying lowest in energy, followed by the $(\pi g_{9/2})^2_{J=2^+} \otimes {}^{88}\text{Sr}_{2^+}$ coupled states. The expected excitation energies for such states can be approximately found from the addition of the ^{88}Sr 2^+ state energy (1836 keV) and the $(\pi g_{9/2})^2_{J=0^+,2^+}$ energies (1761 and 2186 keV, respectively) to be 3.6 and 4.0 MeV. The 2^+ level at 3308 keV showed a transverse form factor in the electron scattering study of Ref. [20], which could only be explained by the presence of $\pi p_{3/2}^{-1} \pi p_{1/2}$ and $\pi f_{5/2}^{-1} \pi p_{1/2}$ transitions. This level was as-

signed [20] as the $(\pi g_{9/2})^2_{J=0^+}\otimes{}^{88}\mathrm{Sr}_{2^+}$ state. If this were a pure configuration, and assuming that there are no components in the $^{88}\mathrm{Sr}_{2^+}$ core state that involve the $\pi g_{9/2}$ configuration, in the weak-coupling limit the $B(E2;[(\pi g_{9/2})^2_{J^+}\otimes{}^{88}\mathrm{Sr}_{2^+}]_{2^+}\rightarrow(\pi g_{9/2})^2_{I_f^\pi})$ values should be equal to $B(E2;2^+_1\rightarrow0^+_{\mathrm{g.s.}})$ of the ^{88}Sr core for $J=I_f$ and be zero otherwise. Examining the decay of the 3308-keV 2^+ state, the dominant decay is to the $(\pi g_{9/2})^2_{2^+}$ state, with a $B(E2;2^+_2\rightarrow2^+_1)$ value of 2.7 ± 0.7 W.u., and weaker decays to the 0^+ states with $B(E2;2^+_2\rightarrow0^+)$ values of 0.44 ± 0.12 and 0.77 ± 0.29 W.u. for the ground state and excited 0^+ state, respectively. This indicates a far more complex structure than that given by $(\pi g_{9/2})^2_{J=0^+}\otimes{}^{88}\mathrm{Sr}_{2^+}$.

One resolution of the above discrepancy is that there is a major component of $(\pi g_{9/2})^2_{J=2^+}$ in the initial-state wave function. Using the $B(E2;2^+_2\rightarrow2^+_1)$ value of 2.7 ± 0.7 W.u., an amplitude of 0.6 is extracted, resulting in a wave function $[0.8(\pi g_{9/2})^2_{J=0^+}+0.6(\pi g_{9/2})^2_{J=2^+}]\otimes{}^{88}\mathrm{Sr}_{2^+}$. While explaining the $2^+_2\rightarrow2^+_1$ decays, this wave function would result in $B(E2;2^+_2\rightarrow0^+)$ values of 2.9 W.u. and 1.6 W.u. for the 0^+_2 and $0^+_{\mathrm{g.s.}}$ levels, respectively, much greater than the values of 0.77 ± 0.29 and 0.44 ± 0.12 W.u. observed experimentally; thus, this mixing of $(\pi g_{9/2})^2$ configurations cannot be solely responsible.

At a higher energy, one may expect a series of levels resulting from the coupling $(\pi g_{9/2})^2_{J=2^+}\otimes{}^{88}\mathrm{Sr}_{2^+}$. In the weak-coupling limit, these should have decays to the $(\pi g_{9/2})^2$, $I_f=2^+$ level with $B(E2)$ values equal to $B(E2;2^+\rightarrow0^+_{\mathrm{g.s.}})$ in ^{88}Sr. At $\approx$4 MeV, there are two levels, with $I^\pi=2^+$ and 4^+, that have enhanced $E2$ decays to the 2186-keV 2^+ level. These transitions have $B(E2)$ values of 6.2 ± 1.4 W.u. and 7.6 ± 3.1 W.u., respectively, in excellent agreement with the expected value of 7.2 ± 0.2 W.u. from the ^{88}Sr core. Further, the 2^+_3 level has no observable decay branch to the 0^+_2 level, while the decay to the ground state is 0.99 ± 0.20 W.u. There is no clear evidence for a pure 0^+ member of the $(\pi g_{9/2})^2_{J=2^+}\otimes{}^{88}\mathrm{Sr}_{2^+}$ configuration; the 0^+ level at 4124 keV was populated very strongly in the two-neutron-transfer reaction and was suggested to be a two-phonon pairing vibration, the strength of which was fragmented over several levels [21]. One of these, namely, the 0^+ level at 4426 keV has a measurable lifetime that leads to $B(E2;0^+\rightarrow2^+_1)=2.1^{+1.3}_{-1.1}$ W.u. This state is assigned as having contributions from the two-phonon pairing vibration and the $(\pi g_{9/2})^2_{J=2^+}\otimes{}^{88}\mathrm{Sr}_{2^+}$ configuration.

E. The $(\pi p_{1/2})^2\pi g_{9/2}\pi p^{-1}_{3/2}$ configuration

The promotion of a proton from the $p_{3/2}$ orbital into the $g_{9/2}$ orbital results in a quadruplet of states with spins 3^- to 6^-. These states can be identified from the results of the $^{93}\mathrm{Nb}(p,\alpha)$ reaction, since the ^{93}Nb target ground state can be described as, in the simplest approximation, $0.75(\pi g_{9/2})^3_{9/2^+}+0.66(\pi p_{1/2})^2\pi g_{9/2}$, with the two $d_{5/2}$ neutrons coupled to zero. In the work of Vergnes *et al.* [4], they identified levels at 3.95, 4.22, 4.28, and 4.54 MeV as resulting from the pickup of a $p_{3/2}$ proton, with the level at 3.95 assigned as a 5^- state. The 4^- level was observed in the (e,e') reaction [20] and in the present work at 4225 keV. The 4534-keV 3^- level has been identified with the 4.54 MeV level in the (p,α) study [4]. Therefore, only the 6^- level remains unassigned. This state was not identified in the present study.

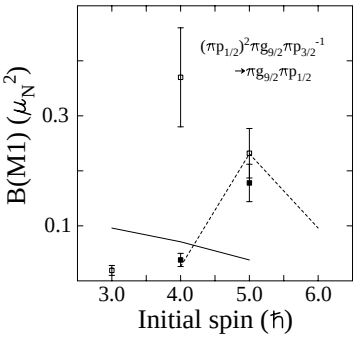

FIG. 8. $B(M1)$ values for decaying transitions from the $(\pi p_{1/2})^2\pi g_{9/2}\pi p^{-1}_{3/2}$ configuration to the $\pi g_{9/2}\pi p_{1/2}$ configuration. The open points and solid line are the experimental and theoretical values, respectively, for decays to the 4^- state, whereas the solid points and the dashed line are those to the 5^- state. The theoretical values were calculated using Eq. (8) with reduced matrix elements from harmonic-oscillator wave functions assuming bare proton g factors.

Decays from the $(\pi p_{1/2})^2\pi g_{9/2}\pi p^{-1}_{3/2}$ configuration to the lower-lying $\pi g_{9/2}\pi p_{1/2}$ configuration involve the one-particle transition $\pi p_{1/2}\rightarrow\pi p_{3/2}$, and thus should have enhanced $B(M1)$ values due to their spin-flip nature. Indeed, this is borne out by the $B(M1;5^-_2\rightarrow4^-_1)$ value of $(0.232\pm0.045)\mu_N^2$ and $B(M1;5^-_2\rightarrow5^-_1)=(0.178\pm0.034)\mu_N^2$ amongst the largest $B(M1)$ values observed in ^{90}Zr.

Using an initial-state wave function of $[[j\otimes j]^{J=0}\otimes[j_1\otimes j_2^{-1}]^{J'}]^{I_i}$, transitions to a final-state configuration of $[j\otimes j_1]^{I_f}$ are given by

$$B(\mathcal{T}^\xi_\lambda;I_i\rightarrow I_f)=\frac{2(2j_2+1)}{2j_1+1}(2I_f+1)\times\begin{Bmatrix} j_1 & j_2 & I_i\\ \lambda & I_f & j\end{Bmatrix}^2|\langle\phi_{j_2}\|\mathcal{T}^\xi_\lambda\|\phi_j\rangle|^2, \quad (8)$$

where ξ labels electric or magnetic transitions. The reduced matrix element $|\langle\phi_{j_2}\|\mathcal{T}^\xi_\lambda\|\phi_j\rangle|$ corresponds to transitions from $j\rightarrow j_2$. In the particular case of the $(\pi p_{1/2})^2\times\pi g_{9/2}\pi p^{-1}_{3/2}\rightarrow\pi g_{9/2}\pi p_{1/2}$ transitions, Eq. (8) predicts that the $5^-_2\rightarrow5^-_1$ $B(M1)$ value should be the largest, a factor of 6 larger than the $5^-_2\rightarrow4^-_1$ $B(M1)$ value. This prediction is contrary to the experimental result, where $B(M1;5^-_2\rightarrow4^-_1)$ is the largest observed. Shown in Fig. 8 are the observed $B(M1)$ values compared to predictions assuming harmonic oscillator wave functions and bare g factors ($g^\pi_s=5.58$, $g^\pi_\ell=1$) for the $(\pi p_{1/2})^2\pi g_{9/2}\pi p^{-1}_{3/2}\rightarrow\pi g_{9/2}\pi p_{1/2}$ transitions. While one expects that the calculated values should be larger

than the experimental results, transitions from the 4_2^- and 5_2^- states to the 4_1^- level are observed to be *much greater* than predicted. The origin of these large $B(M1)$ values is unknown. It must be emphasized here that, especially regarding the $4_2^- \rightarrow 4_1^-$ transition, increasing the multipole mixing does not solve the problem as this would result in an overly large $B(E2)$ value for the transition, which is equally difficult to explain.

F. The $(\pi p_{1/2})^2 \pi g_{9/2} \pi f_{5/2}^{-1}$ configuration

The promotion of a particle from the $\pi f_{f/2}$ orbital to the $\pi g_{9/2}$ orbital results in a series of levels with $I^\pi = 2^- - 7^-$. This configuration could be populated in the (p,α) reaction with $\ell = 3$ transfer. In the work of Vergnes *et al.* [4], levels at 4.36, 4.47, and 5.10 MeV were observed with an angular distribution indicative of $\ell = 3$ transfer. It is also apparent in the high-resolution spectrum published in Ref. [4] that peaks at 4.28 MeV and 4.49 MeV have an $\ell = 3$ component. In the (e,e') reaction, a 6^- level at 4231 keV had a transverse form factor due to the $g_{9/2} f_{5/2}^{-1}$ proton configuration [20]. The negative-parity levels at 4232 keV (6^-), 4299 keV (5^-), 4375 keV (7^-), and 4495 keV (3^-) observed in the present work are suggested as members of the $(\pi p_{1/2})^2 \pi g_{9/2} \pi f_{5/2}^{-1}$ configuration. The 2^- member of the quintuplet is suggested as the 4455-keV $2^{(-)}$ level. The 4299-keV level is suggested to be mixed with the 5^- member of the $(\pi p_{1/2})^2 \pi g_{9/2} \pi p_{3/2}^{-1}$ configuration, leading to its observed $\ell = 1$ transfer component in the (p,α) reaction [4].

In a pure $(\pi p_{1/2})^2 \pi g_{9/2} \pi f_{5/2}^{-1}$ configuration, $M1$ transitions to the $\pi g_{9/2} \pi p_{1/2}$ states would be forbidden. This is, however, not the case as can be seen in Table II. The 4232-keV 6^-, 4299-keV 5^-, and 4495-keV 3^- levels have large $B(M1)$ values for decays to the 4^- or 5^- $\pi g_{9/2} \pi p_{1/2}$ levels, indicating a very significant degree of mixing with the $(\pi p_{1/2})^2 \pi g_{9/2} \pi p_{3/2}^{-1}$ configuration. As is evident from Fig. 8, the large $M1$ strength cannot be explained with the $p_{1/2} \rightarrow p_{3/2}$ transitions solely.

G. The $(\pi g_{9/2})^2 \pi p_{1/2} \pi p_{3/2}^{-1}$ and $(\pi g_{9/2})^2 \pi p_{1/2} \pi f_{5/2}^{-1}$ configurations

Proton particle-hole excitations coupled to the spin-0 coupling of a pair of $g_{9/2}$ protons should also lie at low-excitation energies in ^{90}Zr, in the vicinity of the $(\pi p_{1/2})^2 \otimes p\text{-}h$ states. The $(\pi g_{9/2})^2 \otimes p\text{-}h$ states have positive parity, and thus their identification is more difficult due to the number of other expected positive-parity excitations. The lowest-lying states should be the $[(\pi g_{9/2})^2]_{J=0} \otimes \pi p_{1/2} \pi p_{3/2}^{-1}$ 2^+ and 1^+ levels and the $[(\pi g_{9/2})^2]_{J=0} \otimes \pi p_{1/2} \pi f_{5/2}^{-1}$ 2^+ and 3^+ levels. The $[(\pi g_{9/2})^2]_{J=0} \otimes \pi p_{1/2} \pi p_{3/2}^{-1}$ 2^+ and 1^+ levels may be evident from their expected large $B(M1)$ values for decay to the lower-lying $(\pi g_{9/2})^2$ 0^+ and 2^+ states. The 1^+ level at 4579 keV has a large $B(M1; 1^+ \rightarrow 0_2^+)$ value of 0.19 ± 0.07 μ_N^2, and the 4229-keV 2^+ level has $B(M1; 2^+ \rightarrow 2_1^+) = 0.089 \pm 0.014$ μ_N^2. These levels are thus assigned as arising from the $[(\pi g_{9/2})^2]_{J=0} \otimes \pi p_{1/2} \pi p_{3/2}^{-1}$ configuration. The lack of a clear signature makes the assignment of the 2^+ and 3^+ levels of the $[(\pi g_{9/2})^2]_{J=0} \otimes \pi p_{1/2} \pi f_{5/2}^{-1}$ more difficult, and the only guide is the expectation that they lie close in energy to the $[(\pi g_{9/2})^2]_{J=0} \otimes \pi p_{1/2} \pi p_{3/2}^{-1}$ states. The 3^+ level at 4262 keV is a prime candidate, with the $(1,2^+)$ level at 4237 keV a candidate for the 2^+ member.

H. The $(\pi p_{1/2})^2 \nu d_{5/2} \nu g_{9/2}^{-1}$ configuration

Observed through the single-nucleon-transfer reactions (p,d) [1] and $(^3\text{He},\alpha)$ [2], the $2^+ - 7^+$ levels are also seen in the present study. Lifetimes were obtained for the 2^+, 3^+, 4^+, and 6^+ levels. Except for the 4^+ level, the others have, as expected, rather weak $B(M1)$ and $B(E2)$ values for their decays. The 4^+ level has a surprisingly large $B(M1; 4^+ \rightarrow 4_1^+) = (0.202 \pm 0.034) \mu_N^2$, indicating that it does not have a pure configuration. The origin of this $M1$ strength is unknown.

V. SHELL-MODEL CALCULATIONS

The wave functions for ^{90}Zr were obtained employing the OXBASH code [38] in a model space of $\pi 0 f_{5/2}$, $\pi 1 p_{3/2}$, $\pi 1 p_{1/2}$, and $\pi 0 g_{9/2}$ with the effective Hamiltonian of Ji and Wildenthal (JW) [39]. This Hamiltonian is designed for proton configurations for nuclei with $N = 50$. The starting Hamiltonian was obtained from a two-Yukawa-potential model for the central force. An improved fit to 170 energy data points (ground-state binding energies and excitation energies) for nuclei from ^{82}Ge to ^{96}Pd was obtained by varying 35 linear combinations of the 65 two-body matrix elements in this model space. The experimental energies were reproduced with a rms deviation of 150 keV. The resulting JW Hamiltonian is given in the last column of Table 1 in Ref. [39]. Results for nuclei down to ^{80}Zr obtained with the JW interaction are discussed in Refs. [40] and [41]. The JW Hamiltonian has also been used to calculate electromagnetic transition rates and magnetic moments for $N = 50$ nuclei [42].

The $B(M1)$ and $B(E2)$ values for ^{90}Zr were obtained with multiparticle transition densities combined with single-particle matrix elements as discussed in Ref. [42]. The $E2$ single-particle matrix elements are based on harmonic-oscillator radial wave functions with $\hbar\omega = 8.80$ MeV (a value that gives a rms charge radius close to experiment) and an $E2$ proton effective charge of $e_p = 1.5e$. The $M1$ single-particle matrix elements are obtained with an effective proton spin g factor of 0.7 times the free-nucleon value, and with $g_\ell = 1$ for the orbital g factor. The reduction in the spin g factor comes from a combination of first-order core polarization, higher-order core polarization, and mesonic-exchange corrections to the $M1$ operator. These effective operators are a little different from those used in Ref. [42], but the conclusions that are drawn are qualitative and do not depend on this difference. Note that there are no $E1$ single-particle matrix elements in this model, and that all of the $E1$ strength must come from admixtures of configurations involving orbits outside the model space such as the $0 f_{7/2}$ and $1 d_{5/2}$ orbitals.

Since only proton configurations are employed, it cannot

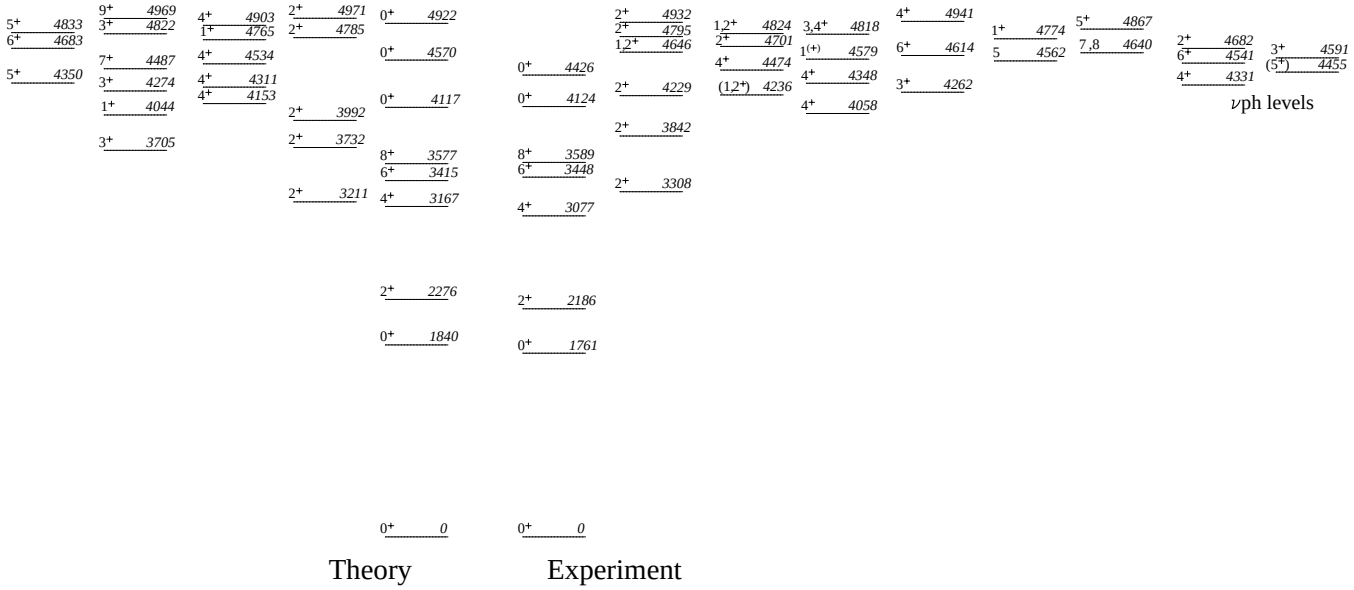

FIG. 9. Spectrum of positive-parity levels predicted (left) by shell-model calculations (using OXBASH described in text) and observed in the present work (right) for ^{90}Zr. Only levels up to 5 MeV are shown. The neutron ph states, labeled on the right side of the plot, have no corresponding levels in the calculations, which used only proton configurations.

be expected that a one-to-one correspondence between observed and calculated levels occurs. However, since the first neutron ph state occurs at ≈4.3 MeV, levels below this should be reasonably explained with the proton configurations, with the caveat that collective components will not be properly accounted for.

Shown in Figs. 9 and 10 are the results of calculations for the positive and negative parities, respectively, compared with the present experimental results. Only levels below 5 MeV are plotted, with the calculated levels on the left and the experimental levels on the right side of the figures. Overall, the calculations reproduce the excited state spectrum well; below 5 MeV, 41 excited states are predicted and 49 are observed, of which five are assigned as neutron ph states and, therefore, should not be considered. Of the 41 predicted levels, 27 are positive parity and 14 negative parity, compared to 29 (seven tentative) positive-parity (not including the neutron ph states) and 16 (two tentative) negative-parity levels observed. The distribution as a function of spin agrees very well, as shown in Fig. 11 for the positive-parity states. The energies of the levels are also well reproduced generally. The most notable exceptions are the 3_1^+ and 1_1^+ levels, which are predicted ≈560 keV lower than observed.

The transition rates do not display the same degree of agreement as the level energies, however. Figure 12 shows the $B(M1)$ values for selected transitions plotted with the abscissa labeled by the state number (the nth occurrence of the level with spin I with increasing excitation energy); only the first five are shown. The calculated values are shown as lines joining the values and the experimental values as data points (where values are known). Detailed agreement should not be expected here since minor adjustments in parameters

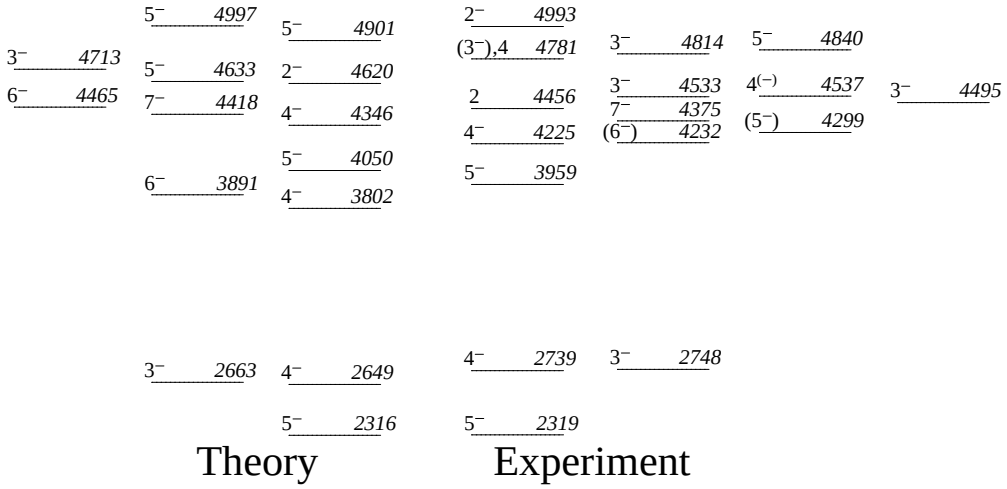

FIG. 10. As in Fig. 9, but for negative-parity states.

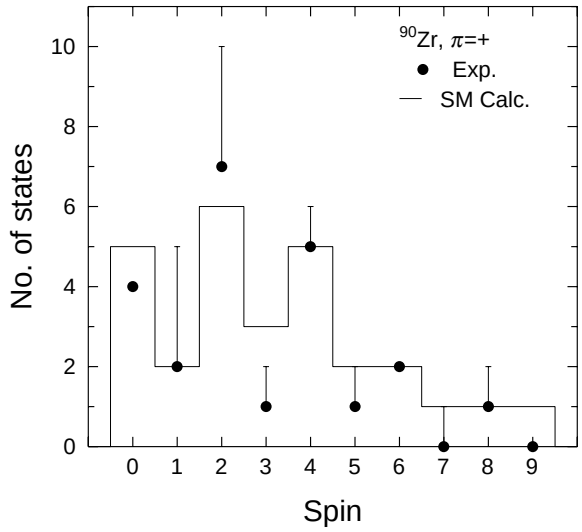

FIG. 11. Distribution of spins predicted by the shell-model calculations (histogram) and experimentally observed (data points) below 5 MeV. The vertical error bar reflects the number of states for which only a range of spins could be given. The neutron ph states are not included in the data.

could result in an interchange of some levels, and further experiments could identify (or clarify) additional levels of a particular spin. What is of interest, rather, are the trends of the experimental and calculated results; do the calculations predict strong transitions whereas experimentally none are found or vice versa? It can be seen, for example, that the 3^- levels have much stronger decays to the 4_1^- and 3_1^- levels than can be accounted for in the calculations; none of the first five levels predicted result in such large $B(M1)$ values. A similar plot for selected $B(E2)$ values, shown in Fig. 13, also reveals some additional discrepancies. Enhanced $E2$ decays from the 2^+ states into the 2_1^+ level are observed, which are not reproduced in the calculations. These particular transitions correspond to states that are assigned as ^{88}Sr core excitations, known to have collective enhancements. Large $B(E2)$ values for the $4_2^- \rightarrow 4_1^-$ and $5_3^- \rightarrow 5_1^-$ transitions also cannot be accounted for, and thus their origin remains unexplained.

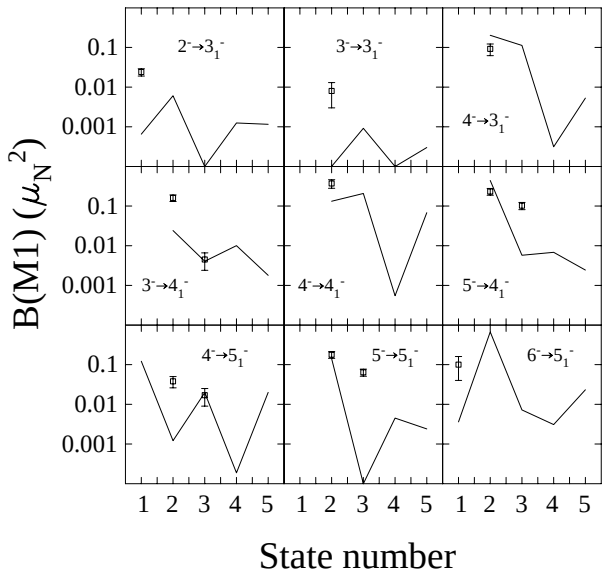

FIG. 12. $B(M1)$ values predicted from shell-model calculations (lines) using OXBASH and observed (data points, as given in Table II), plotted as a function of state number.

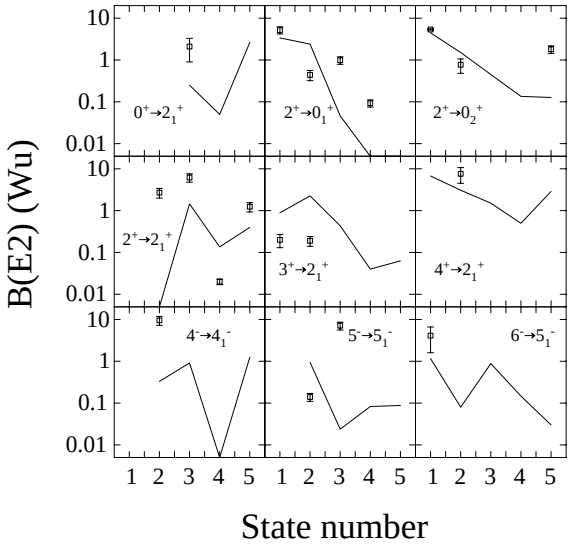

FIG. 13. $B(E2)$ values predicted from shell-model calculations (lines) using OXBASH and observed (data points, as given in Table II), plotted as a function of state number.

An examination of the wave functions predicted shows that they are very complex, and only for the lowest-lying states do single ph components dominate. For example, the lowest 5^- level is dominated by the $\pi g_{9/2}\pi p_{1/2}$ configuration (79%), as suggested in Fig. 6, the second 5^- level by the $(\pi p_{1/2})^2\pi g_{9/2}\pi p_{3/2}^{-1}$ configuration (72%), also consistent with Fig. 6, whereas the third 5^- state has as dominant components 33% $(\pi g_{9/2})^3\pi f_{5/2}^{-1}+23\%$ $(\pi p_{1/2})^2\pi g_{9/2}\pi f_{5/2}^{-1}+13\%$ $(\pi g_{9/2})^3\pi p_{3/2}^{-1}$. As another example, the first 6^- level, suggested to be a member of the $(\pi p_{1/2})^2\pi g_{9/2}\pi f_{5/2}^{-1}$ configuration, has a predicted wave function of 38% $(\pi p_{1/2})^2\pi g_{9/2}\pi f_{5/2}^{-1}+38\%$ $(\pi g_{9/2})^3\pi f_{5/2}^{-1}$ $+11\%$ $(\pi g_{9/2})^3(\pi p_{1/2})^2\pi p_{3/2}^{-2}\pi f_{5/2}^{-1}$. Therefore, it should not be surprising that simple ph configurations used to label the states in the present work cannot describe all details of the levels, such as the transition rates.

VI. SUMMARY

Levels in ^{90}Zr have been investigated using the $(n,n'\gamma)$ reaction with both spallation and monoenergetic neutrons. A detailed level scheme has been constructed, and spin assignments made by consideration of all available data on ^{90}Zr. Lifetimes for many levels have been determined, and transition rates were deduced. Shell-model particle-hole configuration assignments considering ^{88}Sr as a closed core have been suggested for many levels below ≈4.5 MeV. Unexpectedly, large $B(M1)$ and $B(E2)$ values have been observed for

many transitions, which highlight the inadequacy of the simple shell-model configurations suggested here. Shell-model calculations employing a space spanning 12 protons in the fpg shell reproduce the excitation energy spectrum well, but discrepancies arise in detailed comparisons of $B(M1)$ and $B(E2)$ transition rates for individual levels. More detailed studies of ^{90}Zr are clearly needed, including high-resolution (p,α) measurements. Experiments aimed at more precise determinations of the multipole mixing ratios are also required.

ACKNOWLEDGMENTS

This work was performed under the auspices of the U.S. Department of Energy by the University of California, Lawrence Livermore National Laboratory and the Los Alamos National Laboratory under Contract Nos. W-7405-ENG-48 and W-7405-ENG-36, respectively. Work at the University of Kentucky and the Michigan State University were supported by the U.S. National Science Foundation under Grant Nos. PHY-0098813 and PHY-0070911.

[1] J.B. Ball and C.B. Fulmer, Phys. Rev. **172**, 1199 (1968).
[2] H. Fann, J.P. Schiffer, and U. Strohbusch, Phys. Lett. **44B**, 19 (1973).
[3] G. Vourvopoulos and J.D. Fox, Phys. Rev. **177**, 1558 (1969).
[4] M. Vergnes, G. Rotbard, J. Kalifa, and G. Berrier-Ronsin, Phys. Rev. C **10**, 1156 (1974).
[5] E. M. Baum, Ph. D. thesis, University of Kentucky, 1993.
[6] Data extracted using the NNDC On-Line Data Service from the ENSDF database, file revised as of 06/02. M.R. Bhat, in *Evaluated Nuclear Structure Data File (ENSDF)*, edited by S. M. Qaim, Nuclear Data for Science and Technology (Springer-Verlag, Berlin, Germany, 1992), p. 817.
[7] W. Younes (unpublished).
[8] W. Younes, J.A. Becker, L.A. Bernstein, P.E. Garrett, C.A. McGrath, D.P. McNabb, R.O. Nelson, G.D. Johns, W.S. Wilburn, and D.M. Drake, Phys. Rev. C **64**, 054613 (2001).
[9] S.A. Wender, S. Balestrini, A. Brown, R.C. Haight, C.M. Laymon, T.M. Lee, P.W. Lisowski, W. McCorkle, R.O. Nelson, W. Parker, and N.W. Hill, Nucl. Instrum. Methods Phys. Res. A **336**, 226 (1993).
[10] Cross Section Evaluation Working Group, Report BNL-NCS-17451 (ENDF-201), 1991.
[11] P.E. Garrett, N.V. Warr, and S.W. Yates, J. Res. Natl. Inst. Stand. Technol. **105**, 141 (2000).
[12] P.E. Garrett, H. Lehmann, J. Jolie, C.A. McGrath, M. Yeh, W. Younes, and S.W. Yates, Phys. Rev. C **64**, 024316 (2001).
[13] T. Yamazaki, Nucl. Data, Sect. A **3**, 1 (1967).
[14] T. Belgya, G. Molnár, and S.W. Yates, Nucl. Phys. **A607**, 43 (1996).
[15] K.B. Winterbon, Nucl. Phys. **A246**, 293 (1975).
[16] E. Browne, Nucl. Data Sheets **82**, 379 (1997).
[17] L.T. Van Der Bijl, H.P. Blok, J.F.A. Van Hienen, and J. Blok, Nucl. Phys. **A393**, 173 (1983).
[18] E.R. Flynn, A.G. Blair, and D.D. Armstrong, Phys. Rev. **170**, 1142 (1968).
[19] M. Lahanas, D. Rychel, P. Singh, R. Gyufko, D. Kolbert, B. van Krüchten, E. Madadakis, and C.A. Wiedner, Nucl. Phys. **A455**, 399 (1986).
[20] J. Heisenberg, J. Dawson, T. Milliman, O. Schwentker, J. Lichtenstadt, C.N. Papanicolas, J. Wise, J.S. McCarthy, N. Hintz, and H.P. Blok, Phys. Rev. C **29**, 97 (1984).
[21] J.B. Ball, R.L. Auble, and P.G. Roos, Phys. Rev. C **4**, 196 (1971).
[22] H.-W. Muller, Nucl. Data Sheets **54**, 1 (1988).
[23] F.R. Metzger, Phys. Rev. C **9**, 1525 (1974).
[24] E.K. Warburton and D.E. Alburger, Phys. Rev. C **26**, 2595 (1982).
[25] E.K. Warburton, J.W. Olness, C.J. Lister, R.W. Zurmühle, and J.A. Becker, Phys. Rev. C **31**, 1184 (1985).
[26] A.M. van den Berg, E.A. Bakkum, P.W.M. Glaudemans, and D. Zwarts, Phys. Rev. C **29**, 1109 (1984).
[27] R.T. Wagner, E.R. Shunk, and R.B. Day, Phys. Rev. **130**, 1926 (1963).
[28] J.L. Wood, E.F. Zganjar, C. De Coster, and K. Heyde, Nucl. Phys. **A651**, 323 (1999).
[29] R.P. Singhal, S.W. Brian, C.S. Curran, W.A. Gillespie, A. Johnston, E.W. Lees, and A.G. Slight, J. Phys. G **1**, 588 (1975).
[30] R. Liguori Neto, P. Roussel-Chomaz, L. Rochais, N. Alamanos, F. Auger, B. Fernandez, J. Gastebois, A. Gillibert, R. Lacey, A. Miczaika, D. Pierroutsakou, J. Barrette, S.K. Mark, R. Turcotte, Y. Blumenfeld, N. Frascaria, J.P. Garron, J.C. Roynette, J.A. Scarpaci, T. Suomijarvi, A. Van der Woude, and A.M. Van den Berg, Nucl. Phys. **A560**, 733 (1993).
[31] J.R. Beene, D.J. Horen, and G.R. Satchler, Phys. Lett. B **344**, 67 (1995).
[32] B.F. Bayman, A.S. Reiner, and R.K. Sheline, Phys. Rev. **115**, 1627 (1959).
[33] G. Jakob, N. Benczer-Koller, J. Holden, G. Kumbartzki, T.J. Mertzimekis, K.-H. Speidel, R. Ernst, P. Maier-Komor, C.W. Beausang, and R. Krücken, Phys. Lett. B **494**, 187 (2000).
[34] L.B. Horodynski-Matsushigue, G.M. Ukita, T. Borello-Lewin, and J.L.M. Duarte, Phys. Rev. C **60**, 047301 (1999).
[35] B.J. Lund, N.P.T. Bateman, S. Utku, D.J. Horen, and G.R. Satchler, Phys. Rev. C **51**, 635 (1995).
[36] A. Bohr and B.R. Mottelson, *Nuclear Structure* (Benjamin, New York, 1969), Vol. I, p. 83.
[37] N. Auerbach and J.P. Vary, Phys. Rev. C **13**, 1709 (1976).
[38] B.A. Brown, A. Etchegoyen, and W.D.M. Rae, Michigan State University Cyclotron Laboratory Report No. 524, 1985.
[39] X. Ji and B.H. Wildenthal, Phys. Rev. C **37**, 1256 (1988).
[40] X. Ji and B.H. Wildenthal, Phys. Rev. C **40**, 389 (1989).
[41] J.A. Winger, J.C. Hill, F.K. Wohn, R.L. Gill, X. Ji, B.H. Wildenthal, Phys. Rev. C **38**, 285 (1988).
[42] X. Ji and B.H. Wildenthal, Phys. Rev. C **38**, 2849 (1988).